Sleep deprivation soon after recovery from synthetic torpor enhances tau protein dephosphorylation in the rat brain

Sleep deprivation soon after recovery from synthetic torpor enhances tau protein dephosphorylation in the rat brain.

Timna Hitrec[a§], Fabio Squarcio[a§1], Emiliana Piscitiello[a,d], Matteo Cerri[a], Davide Martelli[a,c], Alessandra Occhinegro[a,c], Ludovico Taddei[a,c], Domenico Tupone[a,b], Roberto Amici[a] and Marco Luppi[a,c]*

[a]*Department of Biomedical and NeuroMotor Sciences, University of Bologna, Bologna, Italy.*
[b]*Department of Neurological Surgery; Oregon Health & Science University; Portland, OR – USA.*
[c]*Centre for Applied Biomedical Research – CRBA, University of Bologna, St. Orsola Hospital, Bologna, Italy.*

[§]TH and FS should be considered joint first authors

[1]Present address: Department of Psychiatry, University of Wisconsin-Madison, Madison, WI, USA.

*** Correspondence:**
Dr. Marco Luppi, Department of Biomedical and NeuroMotor Sciences, University of Bologna, Bologna, Italy. Piazza di Porta san Donato, 2 – 40126 Bologna, Italy. Phone number: +390512091731. E-mail: marco.luppi@unibo.it

ORCIDs: TH, 0000-0002-9296-3482; **FS,** 0000-0002-6033-1042; **EP,** 0000-0003-1601-0601; **MC,** 0000-0003-3556-305X; **DM,** 0000-0001-6523-9598; **AO,** 0000-0003-2053-6008; **LT,** 0000-0002-6405-8119; **DT,** 0000-0002-4238-1011; **RA,** 0000-0002-9692-2215; **ML,** 0000-0002-9462-5014

Competing Interests: All authors declare that there are no competing interests for the experiments and results shown in the present paper.

Acknowledgments: The authors wish to thank Ms. Melissa Stott for reviewing the English.

Funding: This work has been supported by the Ministero dell'Università e della Ricerca Scientifica (MUR) – Italy, by the University of Bologna, and with the contribution of: Fondazione Cassa di Risparmio in Bologna and European Space Agency (Research agreement collaboration 4000123556).

Abstract

Neuronal Tau protein hyperphosphorylation (PPtau) is a hallmark of tauopathic neurodegeneration. However, a reversible brain PPtau occurs in mammals during either natural or "synthetic" torpor (ST), a transient deep hypothermic state that can be pharmacologically induced in rats. Since in both conditions a high sleep pressure builds up during the regaining of euthermia, the aim of this work was to assess the possible role of post-ST sleep in PPtau dephosphorylation. Male rats were studied at the hypothermic nadir of ST, and 3-6 hours after the recovery of euthermia, after either normal sleep (NS) or total sleep deprivation (SD). The effects of SD were studied by assessing: i) deep brain temperature (Tb); ii) immunofluorescent staining for AT8 (phosphorylated Tau) and Tau-1 (non-phosphorylated Tau), assessed in 19 brain structures; iii) different phosphorylated forms of Tau and the main cellular factors involved in Tau phospho-regulation, including pro- and anti-apoptotic markers, assessed through western blot in the parietal cortex and hippocampus; iv) systemic factors which are involved in natural torpor; v) microglia activation state, by considering morphometric variations. Unexpectedly, the reversibility of PPtau was more efficient in SD than in NS animals, and was concomitant with a higher Tb, higher melatonin plasma levels, and a higher frequency of the microglia resting phenotype. Since the reversibility of ST-induced PPtau was previously shown to be driven by a latent physiological molecular mechanism triggered by deep hypothermia, short-term SD soon after the regaining of euthermia seems to boost the possible neuroprotective effects of this mechanism.

Keywords: Deep hypothermia; gentle handling; sleep pressure; brain temperature; microglia; melatonin

Non-standard abbreviations list

***aCSF**, artificial cerebrospinal fluid*

***AT8**, Tau protein phosphorylated at S202 and T205*

***C**, control group*

***Hip**, hippocampus*

***IF**, immunofluorescence*

***MI**, morphological index*

***N**, nadir of hypothermia*

***NND**, nearest neighboring distance*

NREMS, *non-rapid eye movement sleep*

***NS,** normal sleep*

***P-Cx**, parietal cortex*

***PPtau**, hyperphosphorylated tau protein*

***R3**, 3h after Tb reached 35,5 °C*

***R3SD**, R3 with total sleep deprivation*

***R6**, 6h after Tb reached 35,5 °C*

***R6SD**, R6 with total sleep deprivation*

REMS, *rapid eye movement sleep*

***RPa**, Raphe Pallidus*

***SD,** sleep deprivation*

***ST,** synthetic torpor*

t, modified t-test*

***Ta**, ambient temperature*

***Tau-1**, Tau protein with no phosphorylation within residues 189-207*

***Tb**, deep brain temperature*

***WB,** western-blot*

Introduction.

Tau protein has the fundamental role of stabilizing microtubules in neurons, ensuring a correct and efficient axonal transport (Wang and Mandelkow, 2016). The main regulatory process for Tau is its phosphorylation (Danis et al., 2019): when phosphorylated, Tau detaches from tubulins, leading to a structural destabilization of microtubules, a fundamental process that allows synaptic plasticity and reorganization to occur (Wang and Mandelkow, 2016). However, when Tau protein is hyperphosphorylated (PPtau), free monomers tend to aggregate into neurofibrillary tangles, the main neuropathological marker that defines tauopathies such as Alzheimer's disease (AD; Goedert and Spillantini, 2019; Maeda and Takashima, 2019). Brain formation of PPtau is also induced in hypothermic conditions, such as hibernation (Arendt et al., 2015) and deep anaesthesia (Whittington et al., 2013), and during a particular deep hypothermic condition that has been pharmacologically induced in the rat (i.e., a non-hibernator; Cerri et al., 2013; Cerri, 2017); this condition has been defined as "synthetic torpor" (ST; Cerri, 2017). In all these conditions, differently from tauopathies or a mouse model of tauopathy (Planel et al., 2009), PPtau Tau hyperphosphorylation is reversible after the recovery of euthermia (Planel et al., 2004; Planel et al., 2007; Arendt et al., 2015; Luppi et al., 2019; Hitrec et al., 2021; Squarcio et al, 2023). We recently demonstrated that the molecular process that leads to PPtau reversibility following ST does not merely follow the passive mechanism classically described by the Arrhenius equations (i.e., with enzymatic activity modifications depending only on changes in brain temperature [cf. Gutfreund, 1995; Marshall, 1997]), but employs an active biochemical and well regulated process. This process is already ongoing during the deep hypothermic condition (and not only during the recovery of euthermia) and is characterized by the phospho-regulation of different brain enzymes and, concomitantly, by a systemic release of melatonin (Squarcio et al., 2023).

It is well known that soon after the return to euthermia following a hypothermic bout, hibernators sleep as if they were sleep deprived (cf. Heller and Ruby, 2004). High sleep pressure was also observed in the rat following ST (Cerri et al., 2013). In particular, during the first few hours after the regain of euthermic conditions, rats showed a high peak in the Delta band (i.e., 0.5-4.5 Hz) of the EEG power spectrum, similarly to that observed during the recovery from prolonged sleep deprivation (SD; Franken et al., 1991; Cerri et al., 2005). Thus, after regaining euthermic conditions, PPtau uniquely returns to normal in concomitance with the occurrence of a deep sleep bout, in either hibernating mammals or rats induced into ST.

The aim of the present work was to investigate whether sleep plays a role in the reversibility of the brain formation of PPtau. To this aim, rats were totally sleep deprived through gentle handling (Franken et al., 1991) soon after their return to euthermia, following the induction of ST; the results were compared to those observed in matched controls that were allowed to sleep. Under these conditions we examined differently phosphorylated forms of Tau protein (Ittner et al., 2016; Wang and Mandelkow, 2016), as well as molecular factors involved in its phospho-regulation (i.e., glycogen-synthase kinase 3β [GSK3β] and protein-phosphatase 2A [PP2A]; Planel et al., 2004; Su et al., 2008). We also planned to determine variations in microglia morphology, as a sign of activation (Ransohoff, 2016; Nilson et al., 2017), and possible functional variations of pro-apoptotic and anti-apoptotic markers factors, in order to verify whether or not SD elicits neurotoxic effects. Finally, we also tested plasma levels of different hormonal factors, involved in stress responses or known to induce possible neuroprotective effects.

Our hypothesis was that SD could make brain PPtau reversibility incomplete or slower. However, in contrast, the results showed that the reversibility of PPtau was more efficient in SD animals than in animals that were allowed to sleep. This enhanced reversibility was concomitant with a higher brain temperature, higher plasma levels of melatonin, and reduced microglia activation. Also, some specific modifications of the

molecular patterns linked to Tau phospho-regulation were observed in SD animals and these modifications were in accordance with a process contrasting the possible PPtau neurotoxicity.

Methods.

Animals

For the experimental conditions "Control", "Nadir of hypothermia", "3h of Recovery", and "6h of Recovery" in the present work the animals used had already been used in the experiment described in Squarcio et al. (2023) (N=24 overall; see later for a better explanation of the experimental conditions), while data from animals used for conditions "3h Recovery Sleep Deprivation" and "6h Recovery Sleep Deprivation" (N=12, overall) have never been published and represent original data for this paper. However, the present work is focused on quantitative "Immunofluorescence", an analysis of the results that was not applied to any experimental condition in our previous paper (Squarcio et al., 2023). However, data from "Western Blots" and "ELISA" analysis and the analysis of "Microglia" related to "3h Recovery" and "6h Recovery" conditions have already been published in the afore-mentioned study and have been repurposed for the present paper in order to allow a comparison with new data from the "3h Recovery Sleep Deprivation" and "6h Recovery Sleep Deprivation" conditions. This choice was made with the intent to better follow the "3-R" ethical rule, reducing the number of animals used as much as possible.
A total of 36 male Sprague–Dawley rats (250-350 gr; Charles River) were used. After their arrival, animals were housed in pairs in Plexiglas cages (Techniplast) under normal laboratory conditions: ambient temperature (Ta) set at 24 ± 0.5◦C; 12h:12h light-dark (LD) cycle (L: 08:00 h–20:00 h; 100–150 lux at cage level); food and water *ad libitum*. All the experiments were conducted following the approval by the National Health Authority (decree: No. 262/2020-PR), in accordance with the DL 26/2014 and the European Union Directive 2010/63/EU, and under the supervision of the Central Veterinary Service of the University of Bologna. All efforts were made to follow the "3-R" ethical rule, minimizing the number of animals used and their pain and distress.

Surgery

After at least one week of adaptation, rats underwent surgery as previously described (Cerri et al., 2013). Briefly, deeply anesthetized rats (Diazepam, 5 mg/kg i.m.; Ketamine-HCl, Imalgene 1000, Merial, 100 mg/kg, i.p.) were placed in a stereotaxic apparatus (David Kopf Instruments) and surgically implanted with: (i) electrodes for the electroencephalogram (EEG); (ii) a thermistor (Thermometrics Corporation) mounted inside a stainless steel needle (21 gauge) and placed beside the left anterior hypothalamus to record the deep brain temperature (Tb); (iii) a microinjection guide cannula (C315G-SPC; Plastics One; internal cannula extension below guide: +3.5 mm), targeted to the brainstem region involved in thermogenic control, the Raphe Pallidus (RPa), at the following coordinates from lambda: 0.0 mm lateral, 3.0 mm posterior and 9.0 mm ventral to the dorsal surface of the cerebellum (Paxinos and Watson, 2007; Morrison and Nakamura, 2019). Since reports have shown that the inhibition of RPa neurons causes vasodilation (Blessing and Nalivaiko, 2001), the increase in tail temperature subsequent to the injection of GABA-A agonist muscimol (1 mM) in RPa was used as proof that the guide cannula was positioned correctly. After surgery, rats received 0.25 ml of an antibiotic solution (penicillin G and streptomycin-sulfate, i.m.), analgesics (Carprofen—Rimadyl, Pfizer—5 mg/kg, i.m.), and 20 ml/kg saline subcutaneously. Animals were constantly monitored until they regained their normal waking behavior and then left to recover for at least 1 week under standard laboratory conditions. Symptoms of the animals' pain, distress, or suffering were constantly evaluated using the Humane End Point (HEP) criteria. 24 hours prior to the experimental session, the rats underwent an

adaptation period in a cage positioned within a thermoregulated and sound-attenuated box, at low Ta (15°C), where the rest of the experimental procedure was carried out.

Synthetic Torpor

To induce ST, we used a consolidated protocol (Cerri et al., 2013; Luppi et al., 2019; Tinganelli et al., 2019; Squarcio et al., 2023). Briefly, a microinjecting cannula was inserted into the previously implanted guide cannula. Then, 100 nl of muscimol (1 mM) was injected once an hour, six consecutive times. Following the last injection, Tb reached values of around 22 °C (Cerri et al., 2013). A control group was injected with artificial cerebrospinal fluid (aCSF; EcoCyte Bioscience). During the whole experiment, EEG and Tb signals were recorded, after being opportunely amplified, filtered, and digitalized (Cerri et al., 2013), with the aim of monitoring sleep behavior and also to better monitor animals' behavior during ST induction and in the following recovery period.

Experimental Procedure

Animals were randomly assigned to six different experimental groups and were sacrificed at different times following the injection of either muscimol or aCSF (first injection at 8.00 a.m.). The experimental groups were the following (Figure 1):

C → Control, injected with aCSF and sacrificed at around 14.00 h, exactly matching the N condition (n = 6).

N → Nadir, sacrificed 1 h after the last injection, at 14:00 h, when Tb reached the nadir of hypothermia (n = 6; Tb = 22.8 ± 1.3 ◦C).

R3 → 3 h Recovery, sacrificed 3 h after the moment in which Tb reached 35.5 °C following ST (i.e., 3h after the moment when animals usually started sleeping), at around 19:00 h (n = 6).

R3SD → 3 h Recovery under total sleep deprivation, exactly matching the timing of R3 (n =6).

R6 → 6 h Recovery, sacrificed 6 h after the moment in which Tb reached 35.5 °C following ST, at around 22:00 h (n = 6).

R6SD → 6 h Recovery under total sleep deprivation, exactly matching the timing of R6 (n =6).

The moment in which Tb reached 35.5 °C during the regaining of euthermia was empirically considered as the end of the hypothermic period, since, in this condition, clearly classifiable sleep reappeared (Cerri et al., 2013).

Total SD was achieved through gentle handling, a well-established and effective procedure to sleep deprive rats by inducing the lowest possible stressful condition (Franken et al., 1991). Handling consisted in the gentle manipulation of the animal by the experimenter when EEG synchronization occurred in order to prevent sleep consolidation. Handling was associated with the introduction of new objects into the cage, which stimulated the curiosity of the animal, thus favoring spontaneous awakening and exploratory activity. As previously described, this procedure is a simple one that allows the animal to be kept awake for more than 90% of the sleep deprivation period (Luppi et al. 2017).

For each experimental group, following deep anesthesia, all animals received a 3-5 ml blood withdrawal by cardiac puncture. Then: i) 3 animals per condition were transcardially perfused with paraformaldehyde 4% (w/v) as previously described (Luppi et al., 2019; Hitrec et al., 2021; Squarcio et al., 2023), in order to collect fixed brain tissue; ii) 3 animals were sacrificed by decapitation, in order to collect fresh brain tissue. Fixed samples were used for immunofluorescence staining, while fresh samples were collected for molecular

assays. Moreover, blood samples were centrifuged at 3000xg at 4°C for 15 min, and plasma was then separated from blood cells and collected for the immuno-enzymatic assays. All samples were stored at -80 °C until assayed.

Wake-sleep states scoring

The procedure has been carried according to standard criteria already described in Cerri et al (2005, 2013). Briefly, sleep stages were visually scored by an operator on the basis of the analysis of the time course of the EEG pattern, the EEG power in the different bands (Delta, 0.5– 4.5 Hz, Theta, 5.0 –9.0 Hz; Sigma, 11.0 –15.0 Hz), and brain temperature, and by using a script developed for Spike2 (sleep score) for the definition or the periods of Wake, non-rapid eye movement sleep (NREMS) and rapid eye movement sleep (REMS) (1-s resolution). The scoring of wake-sleep states has been carried out only for the recovery conditions (i.e., R3, R3SD, R6, R6SD).

Immunofluorescence

The procedure is described in detail in Luppi et al. (2019). Briefly, extracted fixed brains were post-fixed for 2 hours by immersion in the same solution used for the perfusion and put overnight in a 30% (w/v) sucrose solution in phosphate buffer in saline (PBS) and sodium-azide 0.02% (w/v) for cryoprotection (Luppi et al., 2019). Tissue samples were cut into 35 µm-thick coronal slices, using a cryostat-microtome (Frigocut 2800) set at -22.0 °C. All the slices were then stored at −80◦C in a cryoprotectant solution, composed of: 30% (w/v) sucrose, 30% (v/v) ethylene glycol, 1% (w/v) polyvinylpyrrolidone in PBS.

A sample of one out of every six slices of the whole brain was used for immunostaining. Slices were rinsed twice in PBS and then incubated for 2 hours in 1% (v/v) normal donkey serum as a blocking solution. Then, all slices were incubated overnight with the following primary antibodies: i) monoclonal rabbit Anti-NeuN (Merck-Millipore), a neuronal marker; ii) monoclonal mouse Anti-AT8 (Thermo Fisher), marker of the phospho-[Ser202/Thr205]-Tau protein (Malia et al., 2016). Both primary antibodies were diluted at 1:400. Slices were then rinsed twice in PBS with 0.3% (v/v) Triton X-100 and incubated with the following secondary antibodies: i) Donkey Anti-rabbit IgG conjugated with Alexa-488 (Thermo Fisher); ii) Donkey Anti-mouse IgG conjugated with Alexa-594 (Thermo Fisher). Both secondary antibodies were diluted at 1:500. Finally, tissue slices were mounted on coated glass slices and coverslipped with an anti-fade mounting medium (ProLong Gold mountant; Thermo Fisher).

As a control for the AT8 detection, the same procedure was carried out using the monoclonal mouse Anti Tau-1 (Merck-Millipore; 1:400), that detects Tau protein when it has no phosphorylation between residues from 189 to 207 (Szendrei et al., 1993; Billingsley and Kincaid, 1997). The reaction was stained using a Donkey Anti-mouse IgG conjugated with Alexa-594 (1:500).

Microglia activation was also assessed using the rabbit polyclonal Anti-Iba1 antibody (Wako Chemicals; 1:800) and the secondary antibody Donkey Anti-rabbit IgG conjugated with Alexa-594 (Thermo Fisher; 1:500), as previously described. Activation level was measured following established morphometric parameters of microglia cells (Davis et al., 2017; Baldy et al., 2018): i) Soma area; ii) Arborization area; iii) Morphological index (MI): soma area/arborization area ratio; iv) Microglial density (counting the number of cells in every picture taken); v) Nearest neighbor distance. Measurements were carried out by means of ImageJ software, following appropriate calibration.

Finally, endogenous levels of the large fragment (17/19 kDa) of activated caspase-3, resulting from cleavage adjacent to Asp175, were detected using the rabbit polyclonal antibody for Cleaved Caspase-3 (Asp175) (Cell Signaling, 1:300), followed by a Donkey Anti-rabbit IgG conjugated with Alexa-594 (Thermo Fisher; 1:500).

Image acquisition and analysis

Images were obtained using a Leika DMLB microscope equipped with a Nikon DXM 1200 color camera, at 100x magnification (200x for the microglia staining). The composite wide field picture presented in Fig.14 was obtained by manually assembling and editing different microscope fields obtained with an EVOS M5000 Imaging System (Thermo Fisher Scientific).

The number of brain areas analyzed was 19, the same as in the study by Luppi et al. (2019). These brain areas were chosen due to their distribution throughout the whole brain and as representative structures involved in cognitive impairment or in autonomic, temperature, and sleep regulations (Luppi et al., 2019). In a caudal to rostral direction, the analyzed areas were (see Figure 2): nucleus ambiguus (Amb); dorsal motor nucleus of the vagus nerve (dMV); nucleus of the solitary tract (NTS); raphe pallidus (RPa); locus coeruleus (LC); parabrachial nucleus (PBN); ventrolateral part of the periaqueductal grey matter (VLPAG); medial mammillary nucleus (MM); lateral hypothalamus (LH); arcuate nucleus of the hypothalamus (Arc); dorsomedial nucleus of the hypothalamus (DMH); paraventricular nucleus of the hypothalamus (PVH); ventrolateral preoptic nucleus (VLPO); median preoptic nucleus of the hypothalamus (MnPO); paraventricular nucleus of the thalamus (PV); cerebellum cortex (Cb-Cx; not shown in the figure); CA3 field of the hippocampus (CA3); perirhinal cortex (PRh); parietal cortex (P-Cx). The visual recognition of these structures was possible through observation of the NeuN staining (Alexa-488) of the whole section, which was then compared with the atlas schemes.

Fluorescence intensity was determined as described by Chiocchetti and colleagues (2021). Briefly, as in the study by Luppi et al. (2019), during image acquisition from the microscope, the experimenter finely regulated exposure time in order to better reproduce the staining intensity observed through the oculars. Following acquisition, the fluorescence intensity was calculated using the ImageJ software (https://imagej.nih.gov/ij/) and normalized according to the area considered and the background staining intensity. This was calculated by running IF on random brain slices for each experimental condition, using a full protocol but without any primary antibody.

In a previous work, Luppi and colleagues (2019) observed that during the same recovery period as that considered in the present work, i.e., 6h, while AT8 staining was shown to reverse, returning to normal conditions, Tau-1 did not. Since the aim of the present work was to determine whether sleep may affect the return to normal conditions following ST, we here propose the calculation of a “dephosphorylation-index” (DP-Index) as the rate of Tau-1 on AT8 IF intensities in order to better represent the reciprocal phosphorylation states revealed by Tau-1 and AT8 antibodies (Szendrei et al., 1993; Billingsley and Kincaid, 1997; Malia et al., 2016). For each rat, the DP-Index was calculated for each brain structure studied, then averaged into a single value.

Western Blots

After extraction, fresh brains were quickly transferred to a petri dish filled with ice cold PBS. P-Cx and Hip were then isolated, and homogenized by ice-assisted sonication in lysis buffer condition (RIPA Buffer: 50 mM Tris buffer, 150 mM NaCl, 10% (v/v) NP-40, containing a cocktail of protease and phosphatase inhibitors [Sigma-Aldrich], 1 mM dithiothreitol [DTT] and 1 mM PMSF). The extract was centrifuged at 12000xg for 30 min at 4°C and the protein concentration of supenatants was determined using the Bio-Rad DC protein assay kit (Bio-Rad Laboratories) and stored at −80 ◦C. Aliquots were thawed on ice and then denatured in a sample buffer (containing: 500mM DTT, lithium dodecyl sulfate [LDS]) with Coomassie G250 and phenol red; Invitrogen™ NuPAGE) at 65 ◦C for 10 min. Then, protein samples (20 µg) were loaded and separated electrophoretically using a 1.0 mm thick 4 to 12 % Bis-Tris gel together with NuPAGE MOPS SDS Running Buffer (both by Invitrogen™ NuPAGE). The gels were then electrotransferred onto nitrocellulose membranes (Hybond C Extra, Amersham Pharmacia) via wet transfer. Membranes were blocked using 5 % (w/v) not-fat dry milk in 0,1% (v/v) tween-20 in PBS (PBST) for at least 40 min at room temperature, and then incubated overnight at 4 °C with the different primary antibodies indicated in Table 1. Bound antibodies were detected

with horseradish peroxidase-conjugated Anti-rabbit and Anti-mouse secondary antibodies. β-actin was used as a loading control. ChemiDoc™XRS+ (Image Lab™Software, Bio-Rad) was used to acquire digital images through a chemiluminescence reaction (ECL reagents, Amersham). A semi-quantitative measurement of the band intensity was performed using the same computer software and expressed as a ratio of band intensity relative to the loading control.

ELISAs

Plasma samples from six animals for each experimental condition were pooled in order to obtain a sufficient volume to be assessed with all the ELISA kits used and with the aim to reduce the individual variability due to the relatively small number of animals. Therefore, following the pooling we obtained two "grand-samples", each assayed twice independently. Commercially available ELISA kits were used to measure plasma levels of: melatonin (IBL International, RE54021); dopamine (IBL International, RE59161); adrenaline/noradrenaline (IBL International, RE59242); cortisol (IBL International RE52061); corticosterone (Abnova, KA0468). All procedures were run following the manufacturer's recommendations. Optical density was red in a spectrophotometer (Spark® microplate reader, Tecan).

Statistical analysis

The statistical analysis was carried out using SPSS software (25.0), considering $P<0.05$ as the threshold value for significance.

Western blot and ELISA results were analyzed using the Kruskal-Wallis non-parametric test, in the case of significance; every experimental condition mean was compared with the relative C level using the Mann-Whitney non-parametric test.

Deep brain temperature and microglia morphometric results were tested with a 2-way ANOVA, in both cases considering the following main factors: i) time of recovery from ST; ii) sleep condition (i.e., NS or SD). Then, the means of the NS group were compared with the corresponding mean of the SD group, using the modified t-test (t*). All comparisons were independent and α correction was unnecessary.

Wake-sleep amounts were compared considering separately each sleep state (i.e., Wake, NREMS and REMS) and comparing SD groups with the corresponding NS group: R3SD vs. R3; R6SD vs. R6. Results were tested by 1-way ANOVA (main factor: experimental conditions [4 levels]) followed by 2 orthogonal contrasts to compare means.

As previously suggested (Luppi et al., 2019), IF intensities were analyzed following two steps: gross and fine analysis. The gross analysis took into consideration the averaged value of all the brain structures considered for each animal: this analysis was conducted using a one-way ANOVA, when the ANOVA was significant, the means of the different experimental conditions were compared with the relative C level, and each "NS" condition was compared with the relative "SD" condition, using t*. The fine analysis was conducted only considering the recovery periods and focusing on the SD effects (i.e., NS conditions vs. SD conditions). Due to the lack of uniformity of variances, the fine analysis was conducted using non-parametric statistics on each single brain structure: using the Kruskal-Wallis test firstly and, only in the case that this was significant, means were compared using the Mann-Whitney test.

The same non-parametric strategy was also adopted to test differences among conditions for the DP-Index.

Results.

Behavioral data during the Recovery period

Since these parameters were continuously recorded throughout the experimental protocol, both sleep scoring and Tb data related to either R3 or R3SD conditions also include the first 3-h recording of the R6 and R6SD conditions, respectively. Consequently, N=12 for R3 and R3SD and N=6 for R6 and R6SD.

As shown in Table 2, during the recovery period, animals from groups R3 and R6 spent the majority of time sleeping, in accordance with the results described in Cerri et al. 2013, while animals from both the R3SD and R6SD groups spent the large majority of their time awake, as described in the Experimental Procedure section. Results from this analysis presented equal variances among experimental groups. For each sleep state, both the ANOVA main factor was significant (Wake: $F_{(3,32)}$=138.077, df=3, p<0.001; NREMS: $F_{(3,32)}$=128.467, df=3, p<0.001; REMS: $F_{(3,32)}$=40.816, df=3, p<0.001), and all the orthogonal contrasts were significant (p<0.001).

Data related to the modifications of brain temperature (Tb) under the different experimental conditions during the recovery period are shown in Figure 3. Overall, sleep deprived animals showed higher Tb levels than NS animals. Since results from this analysis presented equal variances among experimental groups, a 2-way ANOVA statistic was used, considering the following main factors: i) wake-sleep condition: NS or SD; ii) length of recovery period: 10-minute steps. The "wake-sleep condition" main factor was statistically significant ($F_{(1,35)}$=19.338, df=1, p<0.001). No statistically significant differences were found between recorded values within each 10-min step. It is worth noting that the difference in the levels in Tb that can be observed on passing from the first to the second 3h of the recovery period is due to the different numerosity of the two experimental groups (n=12 and n=6, respectively).

Immunofluorescence for AT8 and Tau-1.

As shown in Luppi et al. (2019), as a first step, data were analyzed without distinguishing between the different brain structures considered in the study (i.e., the "gross analysis"). Then, results were separately analyzed for the 19 brain structures described in Figure 2 (i.e., the "fine analysis"), with a specific focus on the difference between NS and SD groups.

The results of the gross analysis are shown in Figure 4. As expected, in N, AT8 (i.e., the phosphorylated form of Tau protein) IF levels were higher (t*=3.119, df=12, p=0.009), while Tau-1 (i.e., the non-phosphorylated form of Tau protein) IF levels were lower (t*=8.125, df=12, p<0.001) compared to C. However, during the recovery period, while AT8 IF levels returned to C levels, Tau-1 IF levels remained significantly lower than C (t*=6.791, df=12, p<0.001, in R3; t*=7.486, df=12, p<0.001, in R3SD; t*=6.052, df=12, p<0.001, in R6; t*=3.488, df=12, p=0.004, in R6SD), albeit with a non-significant rising trend at R6 and R6SD.

This trend is better represented in Figure 5, reporting the DP-Index. Since Tau-1 and AT8 are antibodies that recognize epitopes that are reciprocally exclusive, we proposed a ratio between their IF levels to indicate the Tau "dephosphorylation level" (DP-index). The results show that the DP-index was largely lower in N compared to C (p=0.0495), moving thereafter to levels closer to C in both R3 and R6, but the value for R6 remained significantly lower than that observed in C (p=0.0495). Moreover, DP-Index levels were significantly affected by SD compared to NS (Kruskal-Wallis test, p=0.029) and, more specifically, they returned close to C levels and were significantly higher than those of the matched NS condition in both R3SD and R6SD (p=0.0495 for both comparisons: R3SD vs. R3 and R6SD vs. R6).

Figure 6 shows the "fine analysis" of IF intensities for all 19 brain regions considered (see Figure 2). For both AT8 and Tau-1 IF levels, 3h after the recovery of euthermia following ST, differences between NS and SD were not statistically significant (Kruskal-Wallis test, N.S. for both). Differently, both the phosphorylated and the de-phosphorylated form of Tau presented differences after 6h of the recovery period (Kruskal-Wallis test,

p=0.0335 for AT8, p=0.0455 for Tau-1). In Panel C of Figure 6, results show that in the SD condition the AT8 IF level was generally lower than that in the NS condition, with statistically significant differences found in: NTS (p=0.0495), dMV (p=0.0495), MM (p=0.0495), DMH (p=0.0495), and CA3 (p=0.0495). Conversely, Panel D shows that in the SD condition higher values of Tau-1 IF levels were observed compared to the NS condition. In the latter case, statistically significant differences were found in: Amb (p=0.0495), dMV (p=0.0495), LC (p=0.0495), Arc (p=0.0495), CA3 (p=0.0495), and P-Cx (p=0.0495). Representative examples of staining intensities of the CA3 field of the hippocampus during the recovery periods, in either NS or SD conditions, are shown in Figure 7.

Western-blot determinations.

For these analyses, as described in the Methods section, the results from rats belonging to the R3 and R6 groups are those taken from the study by Squarcio et al. (2023).

As shown in Figure 8, SD did not induce changes in the concentration of Tau protein in either P-Cx or Hip (Panel A) during the recovery period considered. The same was true for Tau-1 levels, that were unchanged by SD (Panel C). In contrast, Panel B shows that AT8 had lower values in SD conditions compared to NS conditions in P-Cx, although it reached a statistically significant level (p=0.0495) only for R3SD vs. R3. The levels of p[T205]-Tau form are shown in Panel D and were generally higher in SD than in NS conditions, but reached significant levels only in the Hip (p=0.0495 for both comparisons: R3 vs. R3SD and R6 vs. R6SD).

The analysis of the molecular factors involved in the phospho-regulation of Tau protein is shown in Figure 9. In this case, the only statistically significant effects induced by SD were those shown in Panel C: PP2A resulted lower in P-Cx (p=0.0495) and higher in Hip (p=0.0495) in R3SD compared to R3. None of the other molecular factors analyzed showed significant differences.

Figure 10 shows how SD during the recovery period following ST may affect pro-apoptotic, cellular stress, and anti-apoptotic factors: no differences were found in any of the brain structures considered. Also, Figure 11 shows NeuN levels found in P-Cx and Hip at the end of this recovery period, suggesting that SD had no effect on the quantification of this neuronal marker. This supports the lack of any neuronal loss in either P-Cx or Hip 6h after the return to euthermia.

ELISA determinations.

For these analyses, as described in the Methods section, the results from rats belonging to R3 and R6 have been taken from Squarcio et al. (2023).

Figure 12 shows the results from plasma determinations of different systemic factors. Panels A and E show the only statistically different values observed: both melatonin and corticosterone levels were higher in R3SD compared to R3 (p=0.0433, for both melatonin and corticosterone).

Morphometric analysis of microglia in P-Cx and CA3.

For these analyses, as described in the Methods section, the results from rats belonging to R3 and R6 are those found in Squarcio et al. (2023).

Since the results from this analysis presented equal variances among experimental groups, a 2-way ANOVA statistic was used, considering the following main factors: i) length of recovery period: 3h and 6h; ii) wake-sleep condition: sleep allowed (i.e., NS) or SD.

Panels A and B of Figure 13 show the results related to two parameters connected to cell density: the number of cells and their mean distance from each other. For cell number (Panel A), both of the main factors were non-significant, but they significantly interacted with each other in CA3 ($F_{(1,20)}$=13.978, df=1, p=0.001). Also, R3SD presented smaller values compared to R3 in CA3 (t*=3.516, df=20, p=0.002). Considering the “nearest

neighbor distance" (Panel B), while in CA3 the only interaction between factors was significant ($F_{(1,20)}$=11.503, df=1, p=0.003), in P-Cx the "length of recovery period" factor was significant ($F_{(1,20)}$=5.708, df=1, p=0.027) as was the interaction between factors ($F_{(1,20)}$=5.924, df=1, p=0.024). When comparing means between the experimental groups, R3SD values were found significantly different compared to R3 values for both brain structures (t*=2.919, df=20, p=0.008, in CA3; t*=3.141, df=20, p=0.005, in P-Cx).

Panels C, D, and E of Figure 13 show correlated parameters indicating morphological characteristics that strictly represent the functional activation of microglia. Panel D shows that, when analyzing the soma area, no differences resulted from the ANOVA in CA3, while both main factors and their interaction were significant in P-Cx ($F_{(1,20)}$=12.878, df=1, p=0.002, "length of recovery period" factor; $F_{(1,20)}$=9.000, df=1, p=0.007, "wake-sleep condition" factor; $F_{(1,20)}$=6.993, df=1, p=0.016, interaction between factors). Nevertheless, when different experimental groups were compared individually, the mean soma area in R6SD resulted significantly smaller than in R6 for both brain structures (t*=2.547, df=20, p=0.019, in CA3; t*=3.991, df=20, p<0.001, in P-Cx). However, the arborization area analysis, shown in Panel D, presented a significant "length of recovery period" factor for CA3 ($F_{(1,20)}$=5.946, df=1, p=0.024) and P-Cx ($F_{(1,20)}$=19.453, df=1, p<0.001), and a significant interaction between factors in CA3 ($F_{(1,20)}$=21.165, df=1, p<0.001) and P-Cx ($F_{(1,20)}$=24.603, df=1, p<0.001). This parameter was higher in R3SD compared to R3 (t*=2.745, df=20, p=0.012, in CA3; t*=2.113, df=20, p=0.047, in P-Cx), but lower in R6SD compared to R6 (t*=3.761, df=20, p=0.001, in CA3; t*=4.902, df=20, p<0.001, in P-Cx). Panel E shows results for the morphological index, i.e., the ratio between soma and arborization areas. The ANOVA resulted significant only in P-Cx, in particular for the "wake-sleep condition" factor ($F_{(1,20)}$=4.976, df=1, p=0.037) and for the interaction between factors ($F_{(1,20)}$=11.165, df=1, p=0.003). When different experimental groups were compared individually, R3SD was observed to be significantly lower than R3 for both brain structures (t*=2.359, df=20, p=0.029, in CA3; t*=3.940, df=20, p<0.001, in P-Cx).

Figure 14 shows how the microscope fields were considered for the analysis of CA3 and P-Cx (upper panel) and representative examples of microglia morphologies among the different experimental conditions (lower panel), as described by quantitative results in Figure 13.

Discussion.

The results of the present work show that sleep deprivation (SD) during the 6h-period following the recovery of euthermia from synthetic torpor induced a dephosphorylation of Tau protein that was faster than that observed in animals that were allowed to sleep (NS). This more rapid dephosphorylation occurred in concomitance with higher brain temperature levels than those observed in NS animals and was accompanied by modifications of the molecular pattern at both a neuronal and a systemic level, denoting possible neuroprotective effects.

The buildup of high sleep pressure (Heller and Ruby, 2004), as well as the reversibility of the PPtau formation (Arendt et al., 2015) are common findings among hibernating mammals during the regaining of euthermic conditions. Since both features were observed in the ST model (Cerri et al., 2013; Luppi et al., 2019; Squarcio et al., 2023), the possibility that sleep might contribute to favoring the reversibility of PPtau appeared feasible. However, the results from the present work appear not to support this hypothesis, since, overall, sleep appears to slightly slow down the dephosphorylation process in comparison to the rate occurring in the absence of sleep.

The role of sleep during the post-torpid periods has not yet been completely clarified (cf. Cerri et al., 2021). The enhanced slow wave sleep (SWS) observed following torpor bouts and that observed following SD may share many functions, but they also present some differences (Vyazovskiy et al., 2017). In addition, mice, that

are able to enter torpor spontaneously (Hudson and Scott, 1979), show no enhancement of SWS when returning to euthermic conditions following a torpor bout (Lo Martire et al., 2020). However, when considering the EEG spectral analysis, sleep observed following ST appears similar to that observed following SD (Cerri et al., 2013). In terms of natural torpor, this particular sleep period following the recovery from hypothermia has been considered pivotal for the process of recovery of normal cerebral circuit rewiring (Vyazovskiy et al., 2017; Cerri et al., 2017), taking into account that a dramatic, although reversible, retraction of neuronal cell bodies, dendrites, and spines from several cell types has been observed in hibernating ground squirrels during natural torpor (von der Ohe et al., 2007).

It is apparent that the present results do not fully support the former hypothesis. The main role of Tau protein is that of stabilizing microtubules, a role that is better expressed when the protein is not phosphorylated (Wang and Mandelkow, 2016): hence, the lower phosphorylation levels found following SD in our experiments may suggest that in this condition Tau protein stabilizes the microtubule structure better and, consequently, the synaptic remodeling should be reduced compared to normally sleeping animals (Wang and Mandelkow, 2016). On the other hand, the better dephosphorylation of Tau protein may intensify the recovery of a normal axonal transportation and, therefore, result in a better normalization of both neuronal and network functioning (Decker and Mandelkow, 2019). Considering the results obtained in the present study, SD seems to favor a neuroprotective pattern, supporting the latter possibility. In fact, the results show the following molecular pattern: AT8 is lower, p[T205] Tau is higher (that is, a phosphorylated form of Tau that seems to be neuroprotective [Ittner et al., 2016]), and a coherent trend of Akt activation and Gsk3β inhibition (Kitagishi et al., 2014) was also observed. This protective molecular pattern is also corroborated by two other observations from this work: i) levels of melatonin; ii) modifications of microglia. Considering the first point, the higher level of melatonin found in R3SD compared to R3 may play a role in enhancing protective effects: in fact, melatonin stimulates the Akt/Gsk3β antiapoptotic pathway in neurons by acting on MT2 receptors (Liu et al., 2015). Concerning the microglia, the present results show that SD induces mild modifications of the numerical density and of cell morphology, indicating an enhancement of the resting and non-active condition (Davis et al., 2017; Baldy et al., 2018).

Since AT8 and Tau-1 markers react with reciprocally different phosphorylation forms of Tau (cf., Malia et al., 2016; Szendrei et al., 1993), we introduced the DP-Index as an indication of how PPtau evolves toward normality during the recovery period. As described in our first work concerning PPtau formation and resolution in ST (Luppi et al., 2019), while AT8 returned to normal within a few hours, Tau-1 did not. The DP-Index shows a better representation of this observation: the “system” tends to return to normality, but normal index values are far from being reached, as can be seen in the NS groups. A possible explanation could be the persistence of p[T205]-Tau (Squarcio et al., 2023), a phosphorylated pattern of Tau that is not recognized by both markers. This persistence appears to be important, considering the protective effects that p[T205]-Tau may have on neurons (Ittner et al., 2016); however, it is not possible to exclude the concomitant persistence of other phosphorylated forms of Tau protein (Wang and Mandelkow, 2016; Hu et al., 2017). It is worth noting that SD interferes with the DP-Index, inducing a faster return to normal Tau phosphorylation conditions. Again, in terms of the DP-Index, SD appears to induce protective effects for the resolution of brain PPtau following ST.

The fine analysis of the 19 brain structures considered showed how IF effects are detected later in comparison to WB effects: most differences in IF were apparent after 6h of recovery, while most differences in WB were detected after only 3h. Considering these timings and the different sensitivity of the two techniques, it is possible that the molecular modifications described by WB analyses trigger a wider structural modification that is revealed later in the whole structure, detected by the IF. Moreover, as far as the differences in PPtau IF quantifications are concerned, the brain structures that were found to be more greatly affected by SD during the recovery period were almost the same as those found to be more affected by ST itself in the previous analysis from our laboratory (Luppi et al., 2019): i.e., medulla, hypothalamus, and CA3

field of the hippocampus. The heterogeneous PPtau variations among the different brain structures has been already discussed in Luppi et al. (2019), and, since the variability of present data is high, no specific functional implication could be easily speculated on the basis of these results.

Among the many factors studied in the present experiment, Tb appears to play a key role in the dephosphorylation dynamic of Tau protein. The close relationship between the degree of phosphorylation of Tau protein and brain temperature is well established (Whittington et al., 2013; Tournissac et al., 2021). The variation in brain temperature during SD is also consolidated (Franken et al., 1991; Kräuchi, 2007; Luppi et al., 2017; Sela et al., 2021). Recently, the link between AT8 brain levels and temperature variations during the wake-sleep cycle and SD has been described in mice (Guisle et al., 2020): it was shown that brain AT8 levels are clearly temperature-dependent, displaying a reduction during the activity periods and during SD, when the core body temperature is relatively higher. Our results are in line with these findings, since Tb is higher during SD compared to NS conditions, in particular when considering the first 3h of the recovery period (see Fig.3). We have already shown that when rats regain the euthermic condition following ST, as soon as Tb reaches 35.5 °C higher levels in both heart rate and mean arterial pressure compared to the control condition (Cerri et al., 2013) are observed, denoting a sustained sympathetic activity. Therefore, in this condition, when ST is considered to be over (see Fig.1), even though the rats are in a physiological state that is known to be unfavorable to sleep onset (Cerri et al., 2005; Cerri et al., 2017), if left undisturbed they start sleeping, and, what is more, they demonstrate a high EEG delta power activity (Cerri et al., 2013), similarly to the situation observed following prolonged sleep deprivation. The high systemic corticosterone levels observed in the R3SD condition seem to indicate that SD sustains a high degree of sympathetic outflow for a longer period of time, compared to what was described in rats allowed to sleep (Cerri et al., 2013); this may explain the persistence of a higher Tb during the first 3h following the regaining of euthermia. In this scenario, the more intensive PPtau dephosphorylation observed during SD, and in accordance with what sustained by Planel and colleagues (Planel et al., 2004; Planel et al., 2007; Whittington et al., 2013; Guisle et al., 2020; Tournissac et al., 2021; Guisle et al., 2022), brain temperature should have a pivotal role in the reversibility of brain PPtau. However, since SD in rats is strictly linked with both higher brain temperature and higher sympathetic outflow (Luppi et al., 2017), it is difficult to discriminate whether PPtau dephosphorylation is only a matter of brain temperature or whether it may also depend on some physiological mechanism triggered by the sustained autonomic activation. A possible role of Ta in inducing variations of Tb should be excluded in the present experimental procedure, since 28 °C is well below the temperature used in other experiments in which the Ta was manipulated with the specific intent to modify brain temperature (Gao et al., 1995; Guisle et al., 2020). Nevertheless, even though the role of temperature in favoring the dephosphorylation of Tau is well established in literature, the involvement of other factors cannot be excluded and specifically focused experiments should be planned in the future.

Commonly, sleep disturbances are related to the development of tauopathies and dementias (Lew et al., 2021) and this may appear to be in contrast with our results. However, chronic sleep deprivation or sleep disturbances are conditions that are dramatically different from an acute/short term SD (Rechtschaffen et al., 1999; Franken, 2002; Amici et al., 2008); indeed, short term SD may have therapeutic effects for some psychiatric disorders (Giedke and Schwärzler, 2002; Kuhn et al., 2020). Therefore, the present results specifically relate to a short-term SD, during a particular condition in which a high thermogenic activation is concomitant with a sleep onset period. Apart from the hibernating mammals (Heller and Ruby, 2004), to the best of our knowledge ST represented the first description of such a unique condition in a non-hibernator (Cerri et al., 2013).

In conclusion, the parallel between natural torpor and ST is reinforced by the present data compared to existing knowledge. In fact, as already described in mice (Guisle et al., 2020), a species that can enter torpor spontaneously (Hudson and Scott, 1979), the present work shows that the SD during the first few hours after the recovery of euthermia in rats better sustains the reversibility of brain PPtau formation.

The fact that hibernating mammals normally sleep soon after the recovery of euthermia (Heller and Ruby, 2004) indicates that, for some still unknown reason, sleep has a crucial physiological role whatever its apparent negative impact on the rate of Tau dephosphorylation. However, the understanding of the molecular mechanism elicited by SD on this process may have important therapeutic implications. Recent experiments from our lab (Squarcio et al., 2023) suggested that this resolutive process is apparently driven by a latent physiological mechanism that is triggered by deep hypothermia and that starts acting during the hypothermic period. If SD is added as soon as the euthermic condition is regained, the possible neuroprotective effect on the phospho-regulation of Tau protein appears to be further strengthened.

Original data availability

All the original data are accessible upon reasonable request to the Corresponding author. All the images from western-blot analysis are available on AMS Acta, the Open Science repository of the University of Bologna (http://amsacta.unibo.it/id/eprint/6884 - DOI: 10.6092/unibo/amsacta/6884).

References.

Amici R, Cerri M, Ocampo-Garcés A, Baracchi F, Dentico D, Jones CA, Luppi M, Perez E, Parmeggiani PL, Zamboni G (2008). Cold exposure and sleep in the rat: REM sleep homeostasis and body size. Sleep 31:708-715. doi: 10.1093/sleep/31.5.708.

Arendt T, Stieler J, Holzer M (2015). Brain hypometabolism triggers PHF-like phosphorylation of tau, a major hallmark of Alzheimer's disease pathology. J Neural Transm (Vienna) 122:531-539. doi: 10.1007/s00702-014-1342-8.

Baldy C, Fournier S, Boisjoly-Villeneuve S, Tremblay MÈ, Kinkead R (2018). The influence of sex and neonatal stress on medullary microglia in rat pups. Exp Physiol 103:1192-1199. doi: 10.1113/EP087088.

Billingsley ML, Kincaid RL (1997). Regulated phosphorylation and dephosphorylation of tau protein: effects on microtubule interaction, intracellular trafficking and neurodegeneration. Biochem J 323:577-591. doi: 10.1042/bj3230577.

Blessing WW, Nalivaiko E (2001). Raphe magnus/pallidus neurons regulate tail but not mesenteric arterial blood flow in rats. Neuroscience 105:923-929. doi: 10.1016/s0306-4522(01)00251-2.

Cerri M (2017). The Central Control of Energy Expenditure: Exploiting Torpor for Medical Applications. Annu Rev Physiol 79:167-186. doi: 10.1146/annurev-physiol-022516-034133.

Cerri M, Hitrec T, Luppi M, Amici R (2021). Be cool to be far: Exploiting hibernation for space exploration. Neurosci Biobehav Rev 128:218-232. doi: 10.1016/j.neubiorev.2021.03.037.

Cerri M, Luppi M, Tupone D, Zamboni G, Amici R (2017). REM Sleep and Endothermy: Potential Sites and Mechanism of a Reciprocal Interference. Front Physiol 8:624. doi: 10.3389/fphys.2017.00624.

Cerri M, Mastrotto M, Tupone D, Martelli D, Luppi M, Perez E, Zamboni G, Amici R (2013). The inhibition of neurons in the central nervous pathways for thermoregulatory cold defense induces a suspended animation state in the rat. J Neurosci 33:2984-2993. doi: 10.1523/JNEUROSCI.3596-12.2013.

Cerri M, Ocampo-Garces A, Amici R, Baracchi F, Capitani P, Jones CA, Luppi M, Perez E, Parmeggiani PL, Zamboni G (2005). Cold exposure and sleep in the rat: effects on sleep architecture and the electroencephalogram. Sleep 28:694-705. doi: 10.1093/sleep/28.6.694.

Chiocchetti R, Hitrec T, Giancola F, Sadeghinezhad J, Squarcio F, Galiazzo G, Piscitiello E, De Silva M, Cerri M, Amici R, Luppi M (2021). Phosphorylated Tau protein in the myenteric plexus of the ileum and colon of normothermic rats and during synthetic torpor. Cell Tissue Res 384:287-299. doi: 10.1007/s00441-020-03328-0.

Danis C, Dupré E, Hanoulle X, Landrieu I, Lasorsa A, Neves JF, Schneider R, Smet-Nocca C (2019). Nuclear Magnetic Resonance Spectroscopy Insights into Tau Structure in Solution: Impact of Post-translational Modifications. In: Takashima A, WolozinB, Buee L (eds.) Tau Biology. Advances in Experimental Medicine and Biology - vol. 1184. Springer Nature, Singapore, pp 97-103. doi: 10.1007/978-981-32-9358-8_3. ISBN: 978-981-32-9357-1.

Davis BM, Salinas-Navarro M, Cordeiro MF, Moons L, De Groef L (2017). Characterizing microglia activation: a spatial statistics approach to maximize information extraction. Sci Rep 7:1576. doi: 10.1038/s41598-017-01747-8.

Decker JM, Mandelkow EM (2019). Presynaptic Pathophysiology Encoded in Different Domains of Tau – Hyper-Versus Hypoexcitability? In: Takashima A, WolozinB, Buee L (eds.) Tau Biology. Advances in

Experimental Medicine and Biology - vol. 1184. Springer Nature, Singapore, pp 97-103. doi: 10.1007/978-981-32-9358-8_8. ISBN: 978-981-32-9357-1.

Franken P (2002). Long-term vs. short-term processes regulating REM sleep. J Sleep Res 11:17-28. doi: 10.1046/j.1365-2869.2002.00275.x.

Franken P, Dijk DJ, Tobler I, Borbély AA (1991). Sleep deprivation in rats: effects on EEG power spectra, vigilance states, and cortical temperature. Am J Physiol 261:R198-R208. doi: 10.1152/ajpregu.1991.261.1.R198.

Gao BO, Franken P, Tobler I, Borbély AA (1995). Effect of elevated ambient temperature on sleep, EEG spectra, and brain temperature in the rat. Am J Physiol 268:R1365-R1373. doi: 10.1152/ajpregu.1995.268.6.R1365.

Giedke H, Schwärzler F (2002). Therapeutic use of sleep deprivation in depression. Sleep Med Rev 6:361-377. PMID: 12531127.

Goedert M, Spillantini M.G. (2019). Ordered Assembly of Tau Protein and Neurodegeneration In: Takashima A, WolozinB, Buee L (eds.) Tau Biology. Advances in Experimental Medicine and Biology - vol. 1184. Springer Nature, Singapore, pp. 3-21. doi: 10.1007/978-981-32-9358-8_8. ISBN: 978-981-32-9357-1.

Guisle I, Canet G, Pétry S, Fereydouni-Forouzandeh P, Morin F, Kérauden R, Whittington RA, Calon F, Hébert SS, Planel E (2022). Sauna-like conditions or menthol treatment reduce tau phosphorylation through mild hyperthermia. Neurobiol Aging 113:118-130. doi: 10.1016/j.neurobiolaging.2022.02.011.

Guisle I, Gratuze M, Petry S, Morin F, Keraudren R, Whittington RA, Hébert SS, Mongrain V, Planel E (2020). Circadian and sleep/wake-dependent variations in tau phosphorylation are driven by temperature. Sleep 43:zsz266. doi: 10.1093/sleep/zsz266.

Gutfreund H (1995). Kinetics for the Life Sciences: Receptors, Transmitters and Catalysts. Cambridge University Press, Cambridge (UK). ISBN: 0-521-48027-2.

Heller HC, Ruby NF (2004). Sleep and circadian rhythms in mammalian torpor. Annu Rev Physiol 66:275-289. doi: 10.1146/annurev.physiol.66.032102.115313.

Hitrec T, Squarcio F, Cerri M, Martelli D, Occhinegro A, Piscitiello E, Tupone D, Amici R, Luppi M (2021). Reversible Tau Phosphorylation Induced by Synthetic Torpor in the Spinal Cord of the Rat. Front Neuroanat 15, 592288. doi: 10.3389/fnana.2021.592288.

Hu W, Wu F, Zhang Y, Gong CX, Iqbal K, Liu F (2017). Expression of Tau Pathology-Related Proteins in Different Brain Regions: A Molecular Basis of Tau Pathogenesis. Front Aging Neurosci 9:311. doi: 10.3389/fnagi.2017.00311.

Hudson JW, Scott IM (1979). Daily Torpor in the Laboratory Mouse, Mus musculus Var. Albino. Physiological Zoology 52:205-218. doi: 10.1086/physzool.52.2.30152564.

Ittner A, Chua SW, Bertz J, Volkerling A, van der Hoven J, Gladbach A, Przybyla M, Bi M, van Hummel A, Stevens CH, Ippati S, Suh LS, Macmillan A, Sutherland G, Kril JJ, Silva AP, Mackay JP, Poljak A, Delerue F, Ke YD, Ittner LM (2016) Site-specific phosphorylation of Tau inhibits amyloid-β toxicity in Alzheimer's mice. Science 354:904-908. doi: 10.1126/science.aah6205.

Kitagishi Y, Nakanishi A, Ogura Y, Matsuda S (2014). Dietary regulation of PI3K/AKT/GSK-3β pathway in Alzheimer's disease. Alzheimers Res Ther 6:35. doi: 10.1186/alzrt265.

Kräuchi K (2007). The thermophysiological cascade leading to sleep initiation in relation to phase of entrainment. Sleep Med Rev 11:439-451. doi: 10.1016/j.smrv.2007.07.001.

Kuhn M, Maier JG, Wolf E, Mainberger F, Feige B, Maywald S, Bredl A, Michel M, Sendelbach N, Normann C, Klöppel S, Eckert A, Riemann D, Nissen C (2020). Indices of cortical plasticity after therapeutic sleep deprivation in patients with major depressive disorder. J Affect Disord 277:425-435. doi: 10.1016/j.jad.2020.08.052.

Lew CH, Petersen C, Neylan TC, Grinberg LT (2021). Tau-driven degeneration of sleep- and wake-regulating neurons in Alzheimer's disease. Sleep Med Rev 60:101541. doi: 10.1016/j.smrv.2021.101541.

Liu D, Wei N, Man HY, Lu Y, Zhu LQ, Wang, JZ (2015) The MT2 receptor stimulates axonogenesis and enhances synaptic transmission by activating Akt signaling. Cell Death Differ 22:583-596. doi: 10.1038/cdd.2014.195.

Lo Martire V, Berteotti C, Bastianini S, Alvente S, Valli A, Cerri M, Amici R, Silvani A, Swoap SJ, Zoccoli G (2020). The physiological signature of daily torpor is not orexin dependent. J Comp Physiol B 190:493-507. doi: 10.1007/s00360-020-01281-6.

Luppi M, Al-Jahmany AA, Del Vecchio F, Cerri M, Di Cristoforo A, Hitrec T, Martelli D, Perez E, Zamboni G, Amici R (2017). Wake-sleep and cardiovascular regulatory changes in rats made obese by a high-fat diet. Behav Brain Res 320:347-355. doi: 10.1016/j.bbr.2016.12.024.

Luppi M, Hitrec T, Di Cristoforo A, Squarcio F, Stanzani A, Occhinegro A, Chiavetta P, Tupone D, Zamboni G, Amici R, Cerri M (2019) Phosphorylation and Dephosphorylation of Tau Protein During Synthetic Torpor. Front Neuroanat 13:57. doi: 10.3389/fnana.2019.00057.

Maeda S, Takashima A (2019). Tau Oligomers In: Takashima A, WolozinB, Buee L (eds.) Tau Biology. Advances in Experimental Medicine and Biology - vol. 1184. Springer Nature, Singapore, pp 373-380. doi: 10.1007/978-981-32-9358-8_8. ISBN: 978-981-32-9357-1.

Malia TJ, Teplyakov A, Ernst R, Wu SJ, Lacy ER, Liu X, Vandermeeren M, Mercken M, Luo J, Sweet RW, Gilliland GL (2016) Epitope mapping and structural basis for the recognition of phosphorylated Tau by the anti-Tau antibody AT8. Proteins 84:427-434. doi: 10.1002/prot.24988.

Marshall CJ (1997) Cold-adapted enzymes. Trends Biotechnol 15:359-364. doi: 10.1016/S0167-7799(97)01086-X.

Morrison SF, Nakamura K (2019) Central Mechanisms for Thermoregulation. Annu Rev Physiol 81:285-308. doi: 10.1146/annurev-physiol-020518-114546.

Nilson AN, English KC, Gerson JE, Barton Whittle T, Nicolas Crain C, Xue J, Sengupta U, Castillo-Carranza DL, Zhang W, Gupta P, Kayed R (2017) Tau Oligomers Associate with Inflammation in the Brain and Retina of Tauopathy Mice and in Neurodegenerative Diseases. J Alzheimers Dis 55:1083-1099. doi: 10.3233/JAD-160912.

Paxinos G, Watson C (2007) The rat brain in stereotaxic coordinates. 6th Edition. Elsevier, San Diego. ISBN–13: 978-0-12-547612-6.

Planel E, Bretteville A, Liu L, Virag L, Du AL, Yu WH, Dickson DW, Whittington RA, Duff KE (2009) Acceleration and persistence of neurofibrillary pathology in a mouse model of tauopathy following anesthesia. FASEB J 23:2595-2604. doi: 10.1096/fj.08-122424.

Planel E, Miyasaka T, Launey T, Chui DH, Tanemura K, Sato S, Murayama O, Ishiguro K, Tatebayashi Y, Takashima A (2004) Alterations in glucose metabolism induce hypothermia leading to Tau hyperphosphorylation through differential inhibition of kinase and phosphatase activities: implications for Alzheimer's disease. J Neurosci 24:2401-2411. doi: 10.1523/JNEUROSCI.5561-03.2004.

Planel E, Richter KE, Nolan CE, Finley JE, Liu L, Wen Y, Krishnamurthy P, Herman M, Wang L, Schachter JB, Nelson RB, Lau LF, Duff KE (2007) Anesthesia leads to tau hyperphosphorylation through inhibition of phosphatase activity by hypothermia. J Neurosci 27:3090-3097. doi: 10.1523/JNEUROSCI.4854-06.2007.

Ransohoff RM (2016) How neuroinflammation contributes to neurodegeneration. Science 353:777-783. doi: 10.1126/science.aag2590.

Rechtschaffen A, Bergmann BM, Gilliland MA, Bauer K (1999). Effects of method, duration, and sleep stage on rebounds from sleep deprivation in the rat. Sleep 22:11-31. doi: 10.1093/sleep/22.1.11.

Sela Y, Hoekstra MM, Franken P (2021). Sub-minute prediction of brain temperature based on sleep-wake state in the mouse. Elife. 10, e62073. doi: 10.7554/eLife.62073.

Squarcio F, Hitrec T, Piscitiello E, Cerri M, Giovannini C, Martelli D, Occhinegro A, Taddei L, Tupone D, Amici R, Luppi M (2023). Synthetic torpor triggers a regulated mechanism in the rat brain, favoring the reversibility of Tau protein hyperphosphorylation. Front Physiol 14:1129278. doi: 10.3389/fphys.2023.1129278.

Su B, Wang X, Drew KL, Perry G, Smith MA, Zhu X (2008) Physiological regulation of Tau phosphorylation during hibernation. J Neurochem 105:2098-2108. doi: 10.1111/j.1471-4159.2008.05294.x.

Szendrei GI, Lee VM, Otvos L Jr (1993). Recognition of the minimal epitope of monoclonal antibody Tau-1 depends upon the presence of a phosphate group but not its location. J Neurosci Res 34:243-249. doi: 10.1002/jnr.490340212.

Tinganelli W, Hitrec T, Romani F, Simoniello P, Squarcio F, Stanzani A, Piscitiello E, Marchesano V, Luppi M, Sioli M, Helm A, Compagnone G, Morganti AG, Amici R, Negrini M, Zoccoli A, Durante M, Cerri M (2019) Hibernation and Radioprotection: Gene Expression in the Liver and Testicle of Rats Irradiated under Synthetic Torpor. Int J Mol Sci 20:352. doi: 10.3390/ijms20020352.

Tournissac M, Leclerc M, Valentin-Escalera J, Vandal M, Bosoi CR, Planel E, Calon F (2021). Metabolic determinants of Alzheimer's disease: A focus on thermoregulation. Ageing Res Rev 72:101462. doi: 10.1016/j.arr.2021.101462.

von der Ohe CG, Garner CC, Darian-Smith C, Heller HC (2007). Synaptic protein dynamics in hibernation. J Neurosci 27:84-92. doi: 10.1523/JNEUROSCI.4385-06.2007.

Vyazovskiy VV, Palchykova S, Achermann P, Tobler I, Deboer T (2017). Different Effects of Sleep Deprivation and Torpor on EEG Slow-Wave Characteristics in Djungarian Hamsters. Cereb Cortex 27:950-961. doi: 10.1093/cercor/bhx020.

Wang Y, Mandelkow E (2016). Tau in physiology and pathology. Nat Rev Neurosci 17:5-21. doi: 10.1038/nrn.2015.1.

Whittington RA, Bretteville A, Dickler MF, Planel E (2013) Anesthesia and Tau pathology. Prog Neuropsychopharmacol Biol Psychiatry 47:147-155. doi: 10.1016/j.pnpbp.2013.03.004.

Table 1. *Primary antibodies*.

Antibody	Mc/Pc	Host	Target specificity	MW (kDa)	Source and dilution
Anti-Total Tau	Mc	Ms	several Tau protein isoforms between 50-70 kDa	50-70	Merck Millipore; WB 1:5000
Anti-Tau-1	Mc	Ms	non phosphorylated 189-207 residues	52-68	Merck Millipore; WB 1:5000
AT8	Mc	Ms	p-Tau (S202/T205)	68-70	Thermo Fisher; WB 1:1000
Anti-p-Tau (T205)	Pc	Rb	p-Tau (T205)	68-70	Thermo Fisher; IF 1:400; WB 1:1000
Anti-GSK3β	Mc	Rb	GSK3β	46	Cell Signaling Technology; WB 1:3000
Anti-p-GSK3β	Mc	Rb	p-GSK3β (S9)	46	Cell Signaling Technology; WB 1:3000
Anti-Akt	Pc	Rb	Total Akt1, Akt2, Akt3	56-60	Cell Signaling; WB 1:2000
Anti-p-Akt	Pc	Rb	p-Akt1 (S473), p-Akt2 (S473), p-Akt3 (S473)	56-60	Cell Signaling; WB 1:2000
Anti-GRP78	Mc	Rb	GRP78	78	Cell Signaling; WB P-Cx 1:5000; WB Hip 1:3000
Anti-XIAP	Mc	Ms	XIAP	54	Santa Cruz Biotechnology; WB 1:1000
Anti-PP2A Catalytic α	Mc	Ms	PP2A	36	BDT Transduction Laboratories™; WB 1:5000
Anti-cleaved-Caspase 3	Pc	Rb	Cleaved Caspase 3 (A175)	17-19	Cell Signaling; IF 1:300; WB P-Cx 1:250; WB Hip 1:500
Anti-β-actin	Mc	Ms	β-actin	42	Thermo Fisher; WB 1:5000

Mc, monoclonal; **Pc**, polyclonal; **Ms**, mouse; **Rb**, rabbit; **MW**, molecular weight; **p-**, phosphorylated; **IF**, Immunofluorescence; **WB**, Western Blot; **P-Cx**, Parietal cortex; **Hip**, Hippocampus.

Table 2. *Relative time spent in different wake-sleep stages*.

	R3(N=12)	**R3SD**(N=12)	**R6**(N=6)	**R6SD**(N=6)
Wake	**34.41%** *± 4.52%*	**88.98%*** *± 2.28%*	**21.88%** *± 5.50%*	**88.58%*** *± 4.00%*
NREMS	**61.58%** *± 4.09%*	**10.94%*** *± 2.29%*	**72.38%** *± 12.73%*	**11.42%*** *± 4.00%*
REMS	**4.00%** *± 0.91%*	**0.00%*** *± 0.00%*	**5.74%** *± 1.20%*	**0.00%*** *± 0.00%*

R3, R6, 3h or 6h of recovery, respectively, following synthetic torpor (see methods for details); **R3SD, R6SD**, 3h or 6h of recovery following synthetic torpor, respectively, with a total sleep deprivation (see methods for details); **NREMS,** non-REM sleep; **REMS**, REM sleep. Values are expressed as means ± SEM. Number of animals are indicated near the experimental condition. * SD vs. NS ($P<0.05$).

Figure captions.

Figure 1. Schematic representation of the experimental plan. The solid line indicates the progress of deep brain temperature (Tb) during the experimental procedure. The dotted line refers to the control group (C; i.e., injected with artificial cerebrospinal fluid). The shaded area represents the induction of synthetic torpor (ST) by injecting muscimol within the Raphe Pallidus. N, the nadir of hypothermia during ST; R3, samples taken 3h after Tb reached 35.5 °C following ST; R6, samples taken 6h after Tb reached 35.5 °C following ST. R3SD and R6SD are the same as R3 and R6, respectively, with total sleep deprivation. See Methods for details.

Figure 2. Schematic representation of the brain areas analyzed. Bregma level is reported near each representation. See Methods section for more details. *3V*, third ventricle; *ac*, anterior commissure; *Amb*, nucleus ambiguus; *Aq*, Sylvius aqueduct; *Arc*, arcuate nucleus of the hypothalamus; *CA3*, field CA3 of the hippocampus; *DMH*, dorsomedial nucleus of the hypothalamus; *dMV*, dorsal motor nucleus of the vagus nerve; *LC*, locus coeruleus; *LH*, lateral hypothalamus; *mCP*, middle cerebellar peduncle; *MM*, medial mammillary nuclei; *MnPO*, median preoptic nucleus of the hypothalamus; *NTS*, nucleus of the solitary tract; *ot*, optic tract; *PBN*, parabrachial nucleus; *P-Cx*, parietal cortex; *PRh*, perirhinal cortex; *PV*, paraventricular nucleus of the thalamus; *PVH*, paraventricular nucleus of the hypothalamus; *py*, pyramidal tract; *RPa*, raphe pallidus; *VLPAG*, ventrolateral part of the periaqueductal grey matter; *VLPO*, ventrolateral preoptic nucleus. The cerebellum is not represented.

Figure 3. Representation of the evolution of deep brain temperature (Tb) during the 6h recovery period following synthetic torpor (ST). The temperature was measured within the anterior hypothalamus, see Methods for details. The black line represents normal sleep group (NS; i.e., allowed to sleep during the recovery period), the gray line represents the sleep-deprived group (SD; i.e., subjected to gentle handling throughout the whole period). Since Tb was continuously recorded, for the first 3h N=12, while for the rest of the period N=6: the dashed vertical line represents this transition. Data are represented as means ± S.E.M. for 10-minute time intervals. #, $P < 0.05$ NS/SD main factor 2-way ANOVA test.

Figure 4. Results from the immunofluorescence (IF) quantifications. Staining intensities are normalized in relation to the area considered for each slide and for the background level (see Methods section for details). As a "gross analysis", histograms show averaged values considering all the 19 brain structures studied, put together. In red are the IF intensities for AT8 (i.e., p[S202/T205]-Tau), in blue the IF intensities for Tau-1 (i.e., the non-phosphorylated form of Tau protein). Data are represented as means ± S.E.M. C, control group; N, the nadir of hypothermia during ST; R3, samples taken 3h after Tb reached 35.5 °C following ST; R6, samples taken 6h after Tb reached 35.5 °C following ST. R3SD and R6SD are defined similarly to R3 and R6, respectively, but with the addition of a total sleep deprivation. *, $P < 0.05$ vs. C.

Figure 5. Considering the "gross analysis" results represented in Figure 4, here the results are shown as the rate of immunofluorescence (IF) quantifications of Tau-1 (i.e., the non-phosphorylated form of Tau protein) relatively to IF quantifications of AT8 (i.e., p[S202/T205]-Tau), for each rat and during the whole experimental plan (see Figure 1). This rate has been designated as the "dephosphorylation-index" (DP-Index). The black line represents the resulting DP-Index in the common first experimental conditions (i.e., control [C] and the nadir of hypothermia [N] during synthetic torpor [ST]) and in the recovery period which follows ST, with normal sleep (NS) allowed. The gray line represents the resulting DP-Index solely in the recovery period following ST, with total sleep deprivation (SD). Data are represented as means ± S.E.M. R3, samples taken 3h after deep brain temperature (Tb) reached 35.5 °C following ST; R6, samples taken 6h after Tb reached 35.5 °C following ST. *, $P < 0.05$ vs. C; #, $P < 0.05$ Kruskal-Wallis test; @, $P < 0.05$ NS vs. SD.

Figure 6. Immunofluorescence (IF) quantifications. The graphs show results for each of the 19 structures analyzed, comparing animals that were allowed to sleep normally (NS; black lines) with animals that were totally sleep deprived (SD; gray lines), during recovery from synthetic torpor. Staining intensities are normalized in relation to the area considered for each structure and for the background level (see Methods section for details). Panels A and C represent IF intensities of AT8 (i.e., p[S202/T205]-Tau), for 3h or 6h of recovery from ST (i.e., R3 or R6 conditions), respectively. Panels B and D represent IF intensities of Tau-1 (i.e., non-phosphorylated Tau protein), for R3 or R6, respectively. See Figure 1 for the experimental conditions and Figure 2 for brain structure abbreviations. Data are represented as means ± S.E.M. *, $P < 0.05$ NS vs. SD; #, $P < 0.05$ Kruskal-Wallis test.

Figure 7. Representative pictures showing the CA3 field of the hippocampus. For the left panel, the green column represents NeuN staining (neuronal maker, secondary conjugated with Alexa-488) and the red column represents AT8 staining (phosphorylated Tau, secondary conjugated with Alexa-594). For the right panel, the green column represents NeuN staining (secondary conjugated with Alexa-488) and the red column represents Tau-1 staining (non-phosphorylated Tau, secondary conjugated with Alexa-594). Samples from R3 rats that were allowed to sleep were taken 3h after deep brain temperature (Tb) reached 35.5 °C following ST; R3SD denotes the same experimental time as R3, but with animals being totally sleep deprived; R6 rats were allowed to sleep and samples were taken 6h after Tb reached 35.5 °C following ST; R6SD underwent the same experimental time as R6, but were totally sleep deprived. Calibration bar: 100µm.

Figure 8. Western Blot (WB) quantifications of Total Tau and dephosphorylated/phosphorylated Tau protein levels in brain extracts of the parietal cortex (P-Cx) and hippocampus (Hip). Below each histogram is the WB representative sample for each experimental condition. Panel A: Total Tau protein; Panel B: AT8 (phosphorylated Tau at Ser202/Thr205); Panel C: Tau-1 (Tau protein dephosphorylated at 189-207 residues); Panel D: p[T205]-Tau (phosphorylated Tau at Thr205). Data are normalized by β-actin and expressed as a mean ± SE, n = 3. *: $p < 0.05$, sleep-deprived conditions vs. the respective normal-sleep condition. Experimental groups: R3, samples taken 3 h after Tb reached 35.5 °C following ST; R3SD, the same experimental time as R3, but totally sleep deprived; R6, samples taken 6 h after Tb reached 35.5 °C following ST; R6SD, the same experimental time as R6, but totally sleep deprived.

Figure 9. Western Blot (WB) quantifications of the main enzymes involved in the phospho-regulation of Tau protein expressed in brain extracts of the parietal cortex (P-Cx) and hippocampus (Hip). The WB representative sample for each experimental condition is shown below each histogram. Panel A: Gsk3β, glycogen-synthase kinase 3β (i.e., the main kinase acting on Tau protein); Panel B: p[S9]-Gsk3β (inactive form of Gsk3β, phosphorylated at Ser9); Panel C: PP2A, protein-phosphatase 2A (i.e., the main phosphatase acting on Tau protein); Panel D: Akt 1/2/3 isoforms (i.e., an anti-apoptotic factor, also known as protein-kinase B, with kinase activity on Gsk3β); Panel E: p[S473]-Akt, the active form of Akt, phosphorylated at Ser473. Data are normalized by β-actin and expressed as a mean ± SE, n = 3. *: $p < 0.05$, sleep-deprived conditions vs. the respective normal-sleep condition. Experimental groups: R3, samples taken 3 h after Tb reached 35.5 °C following ST; R3SD, the same experimental time as R3, but totally sleep deprived; R6, samples taken 6 h after Tb reached 35.5 °C following ST; R6SD, the same experimental time as R6, but totally sleep deprived.

Figure 10. Western Blot (WB) quantifications of pro- and anti- apoptotic and cell-stress factors in brain extracts of the parietal cortex (P-Cx) and hippocampus (Hip). Below each histogram is the WB representative sample for each experimental condition. Panel A: cleaved-caspase 3 (apoptotic factor, activated by cleaving at Asp175); Panel B: GRP78, Glucose regulating protein 78 (marker of cellular stressed conditions); Panel C: XIAP, X chromosome-linked inhibitor of apoptosis. Data are normalized by β-actin and expressed as a mean ± SE, n = 3. *: $p < 0.05$, sleep-deprived conditions vs. the respective normal-sleep condition. Experimental groups: R3, samples taken 3 h after Tb reached 35.5 °C following ST; R3SD, the same experimental time as

R3, but totally sleep deprived; R6, samples taken 6 h after Tb reached 35.5 °C following ST; R6SD, the same experimental time as R6, but totally sleep deprived.

Figure 11. Western Blot (WB) determinations of NeuN levels (i.e., neuronal marker) in brain extracts of the parietal cortex (P-Cx) and hippocampus (Hip). Below each histogram is the WB representative sample for each experimental condition. Data are normalized by β-actin and expressed as a mean ± SE, n = 3. *: $p < 0.05$ vs. C. Experimental groups: C, control; R6, samples taken 6 h after Tb reached 35.5°C following ST; R6SD, the same experimental time as R6, but totally sleep deprived.

Figure 12. Levels of different plasmatic factors. Panel A: Melatonin; Panel B: Adrenaline; Panel C: Noradrenaline; Panel D: Dopamine; Panel E: Corticosterone; Panel F: Cortisol. Data are expressed as means ± SE. *: $p < 0.05$, sleep-deprived conditions vs. the respective normal-sleep condition. Experimental groups: R3, samples taken 3 h after Tb reached 35.5 °C following ST; R3SD, the same experimental time as R3, but totally sleep deprived; R6, samples taken 6 h after Tb reached 35.5 °C following ST; R6SD, the same experimental time as R6, but totally sleep deprived.

Figure 13. Morphometric results from the microglia analysis, considering the CA3 field of the hippocampus and the parietal cortex (P-Cx). R3, samples taken 3h after deep-brain temperature (Tb) reached 35.5 °C following synthetic torpor (ST); R6, samples taken 6h after Tb reached 35.5 °C following ST. R3SD and R6SD are defined similarly to R3 and R6, respectively, but with the addition of a total sleep deprivation. Panel A shows results from cell counting within the acquisition frame; Panel B shows results for the "nearest neighbor distance", the mean distance among neighboring cells; Panel C shows results from the mean area of microglia somas; Panel D shows results from the mean microglia arborization; Panel E shows results from the "morphological index", defined as the rate of soma area/arborization area. Data are shown as means ± S.E.M. Beside each panel are the results of the 2-way ANOVA test, showing the main factor effects as well as their

possible statistical interaction. *, $P < 0.05$ SD vs. normal sleep (NS); §, $P < 0.05$ for main factors or their interaction.

Figure 14. Representative sample pictures stained for Iba-1 (secondary conjugated with Alexa-594), a specific microglia marker, from results shown in Figure 13. Pictures are taken with a 200X magnification. The top panel is a composite picture, stained for the pan-neuronal marker NeuN (secondary conjugated with Alexa-488), showing the localization of the brain areas analyzed in a wide field (Red calibration bar: 200μm.). R3, samples taken 3h after deep-brain temperature (Tb) reached 35.5 °C following synthetic torpor (ST); R6, samples taken 6h after Tb reached 35.5 °C following ST. R3SD and R6SD are defined similarly to R3 and R6, respectively, but with the addition of a total sleep deprivation. The inclusions within panels show a typical example of microglial cell morphology for that specific experimental condition, at a higher magnification. White calibration bar: 50μm.

Figure 1

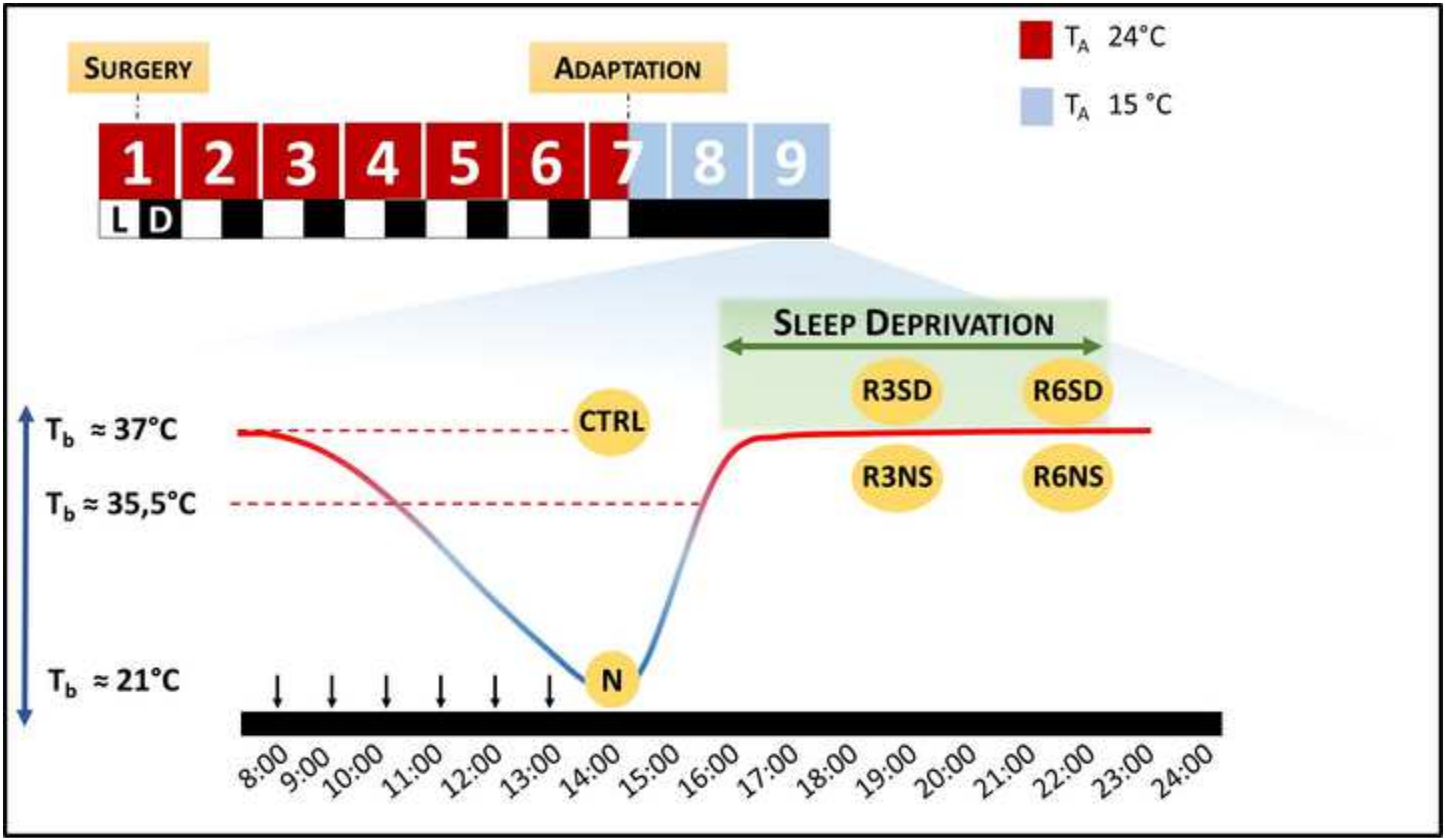

Figure 2

Click here to access/download;Figure;Hitrec-Squarcio et al_Figure 2.jpg

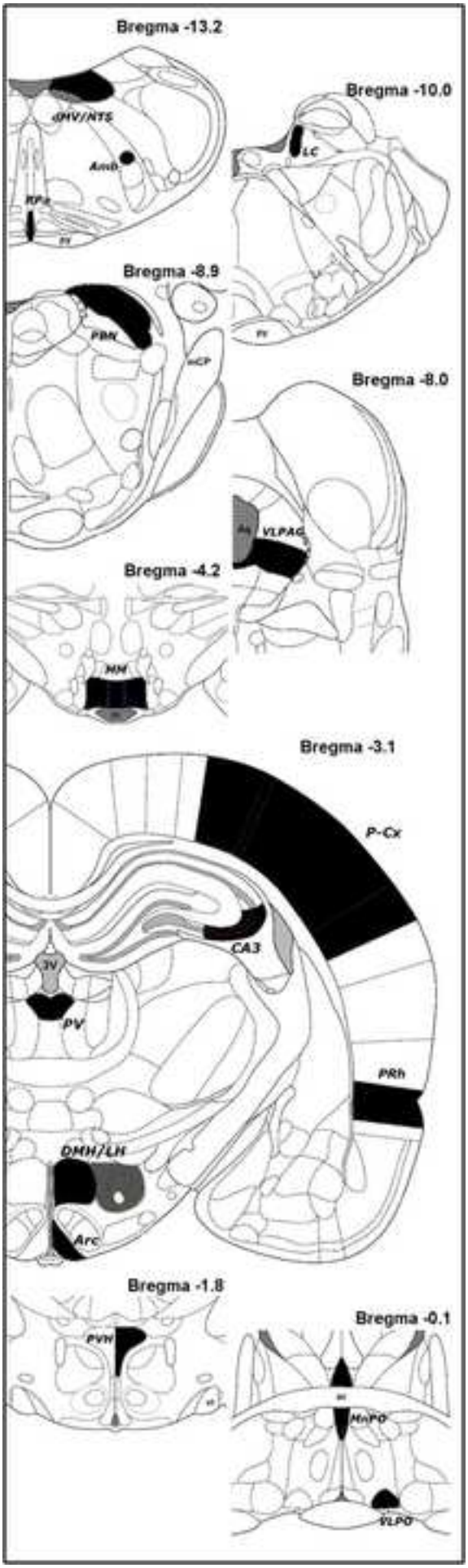

Figure 3

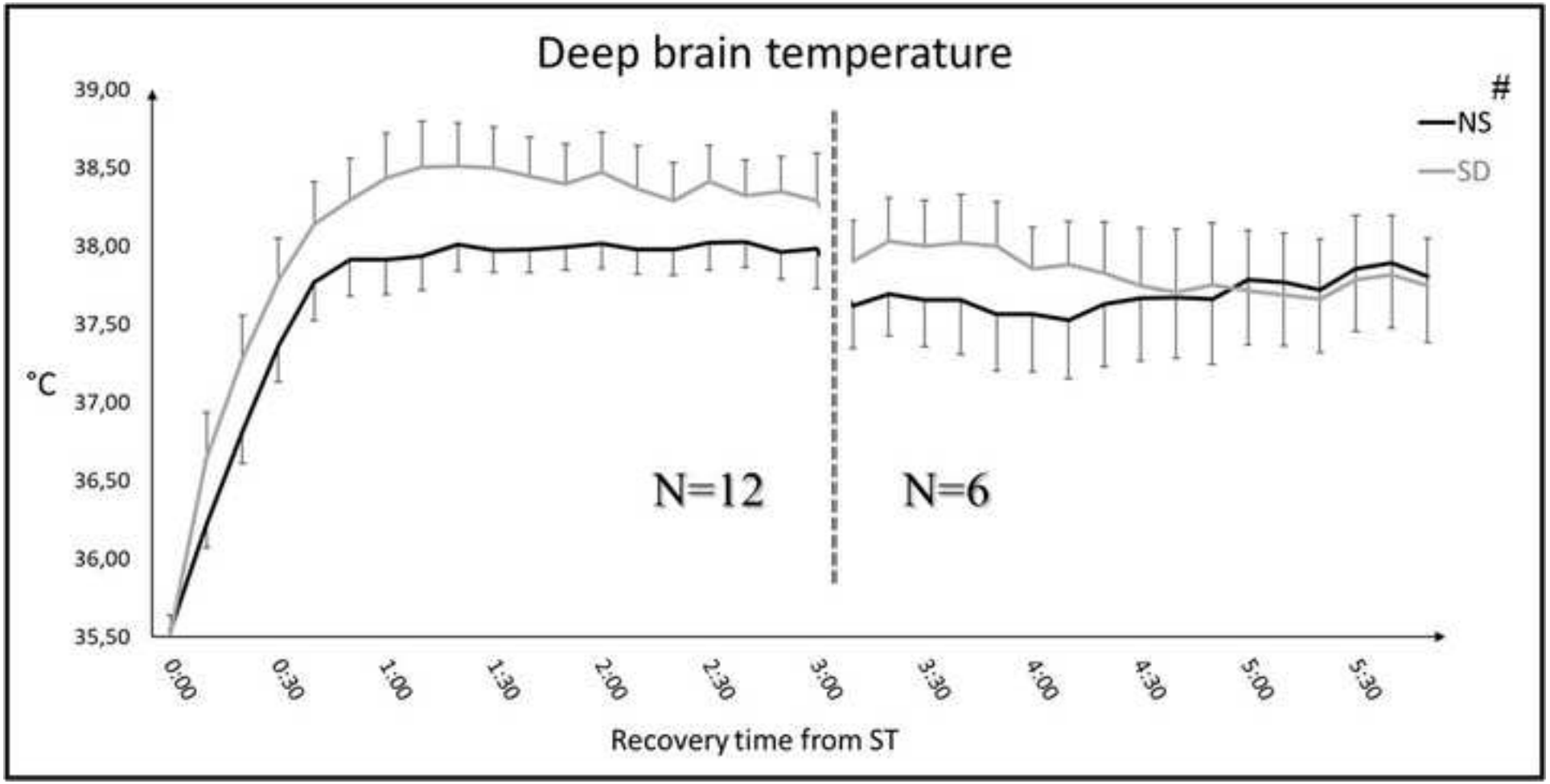

Figure 4

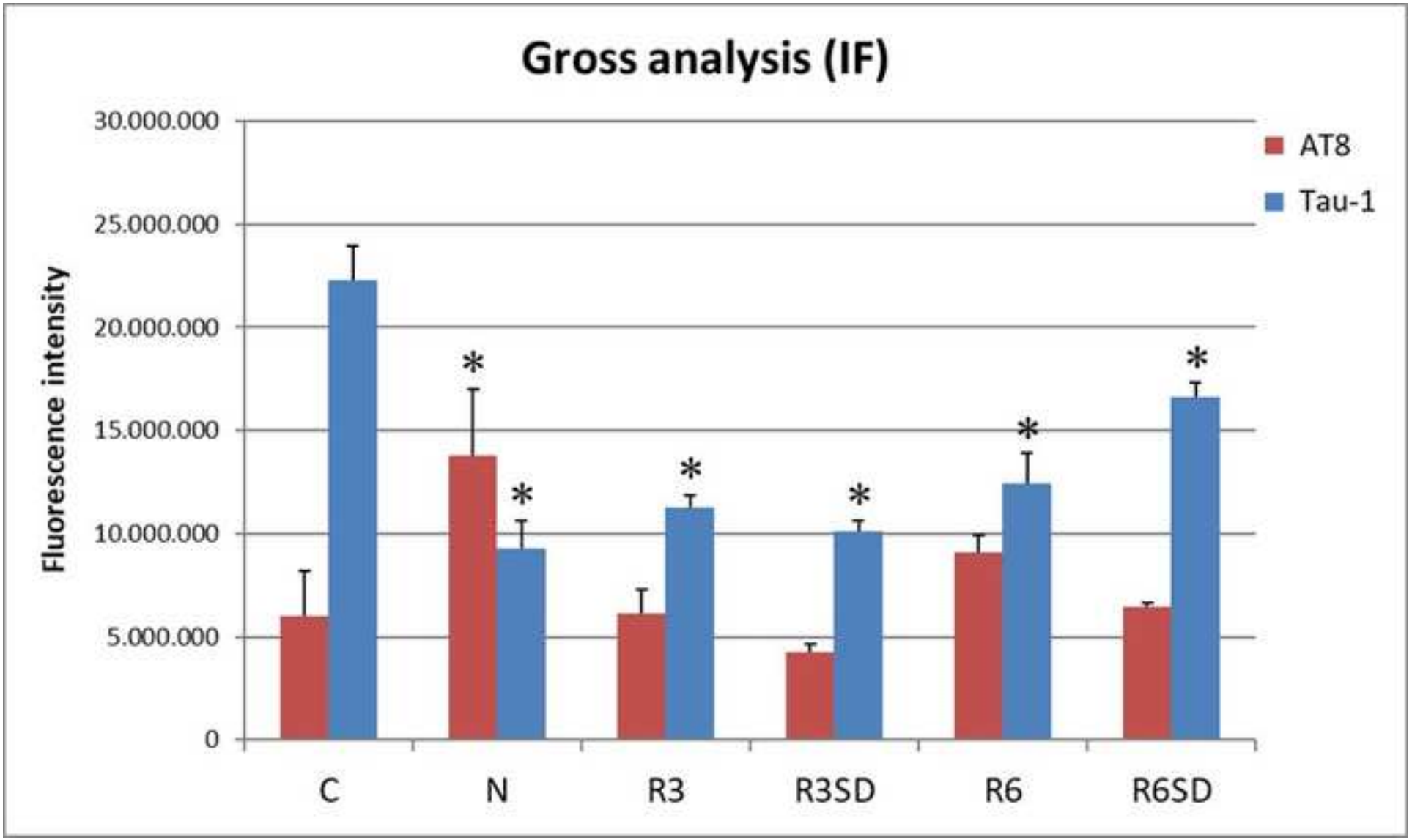

Figure 5

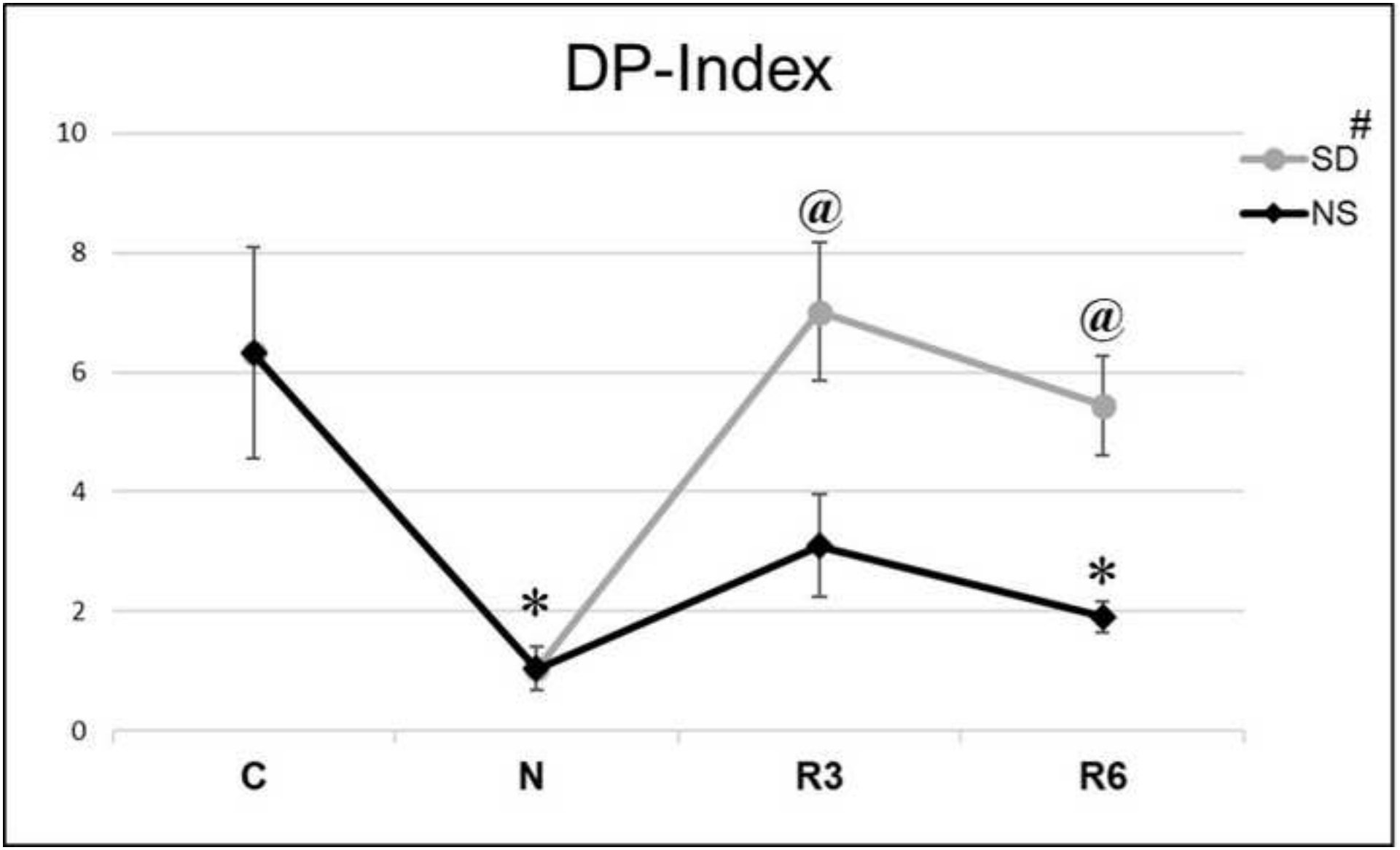

Figure 6

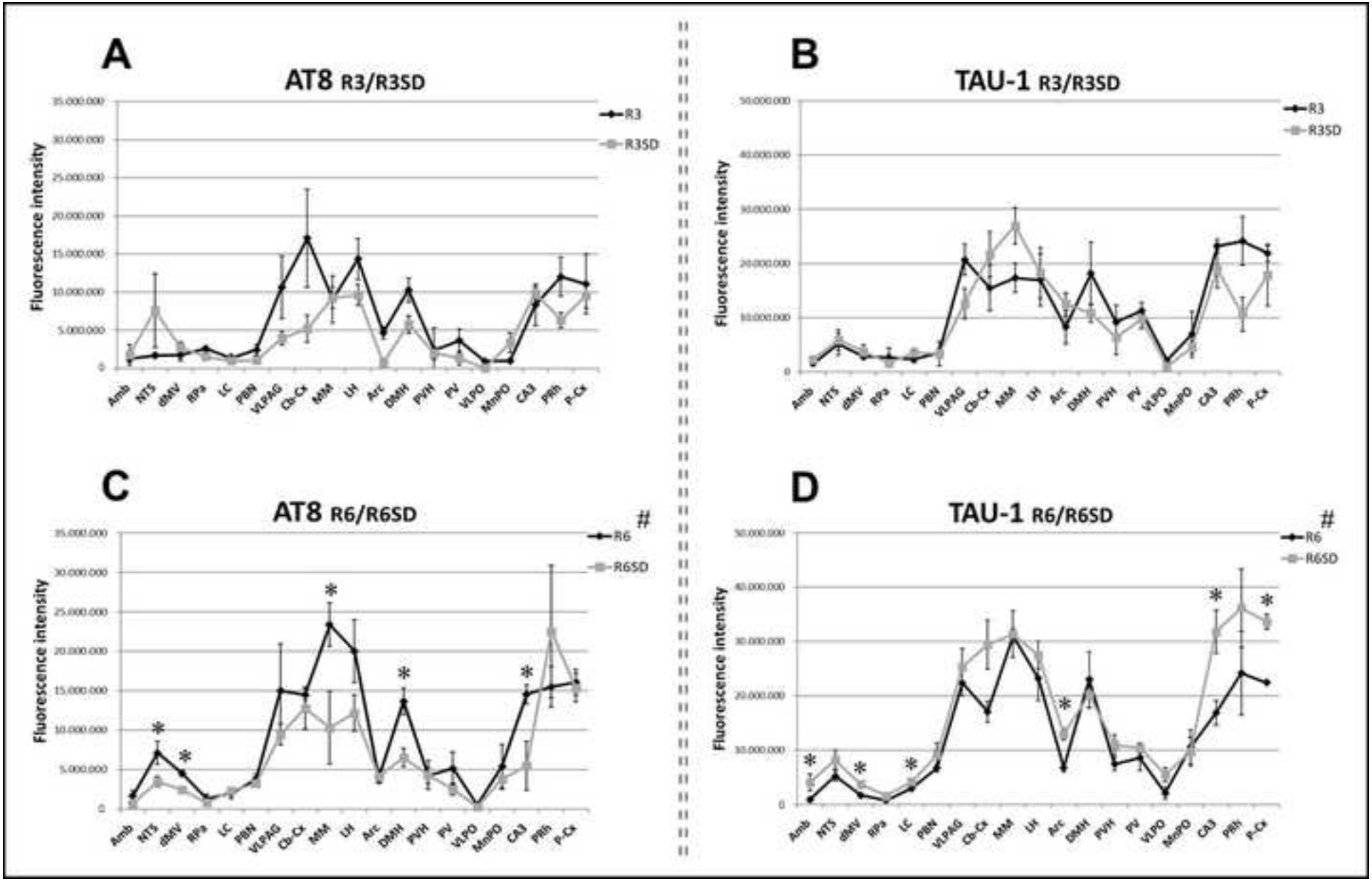

Figure 7

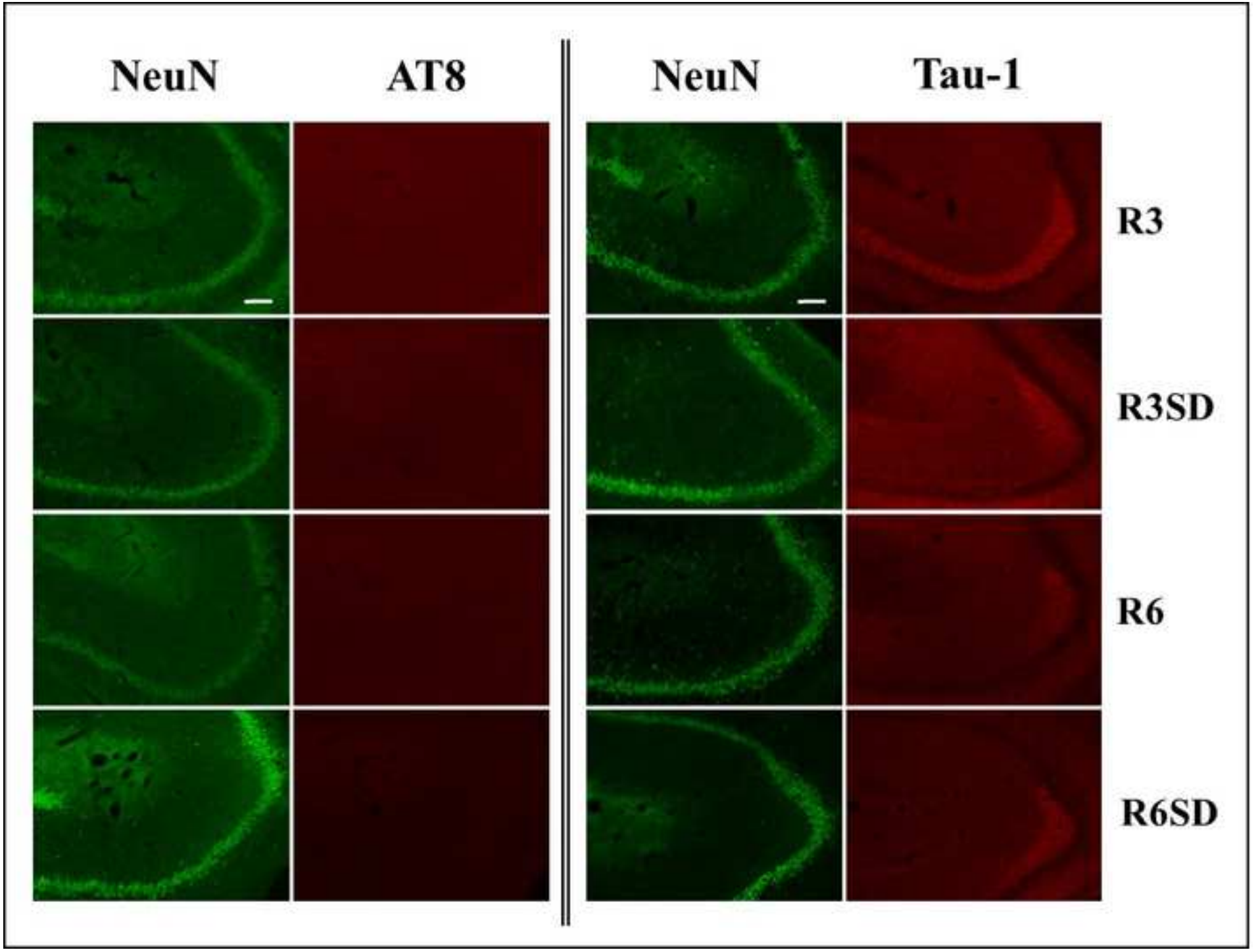

Figure 8

Click here to access/download;Figure;Hitrec-Squarcio et al_Figure 8.jpg

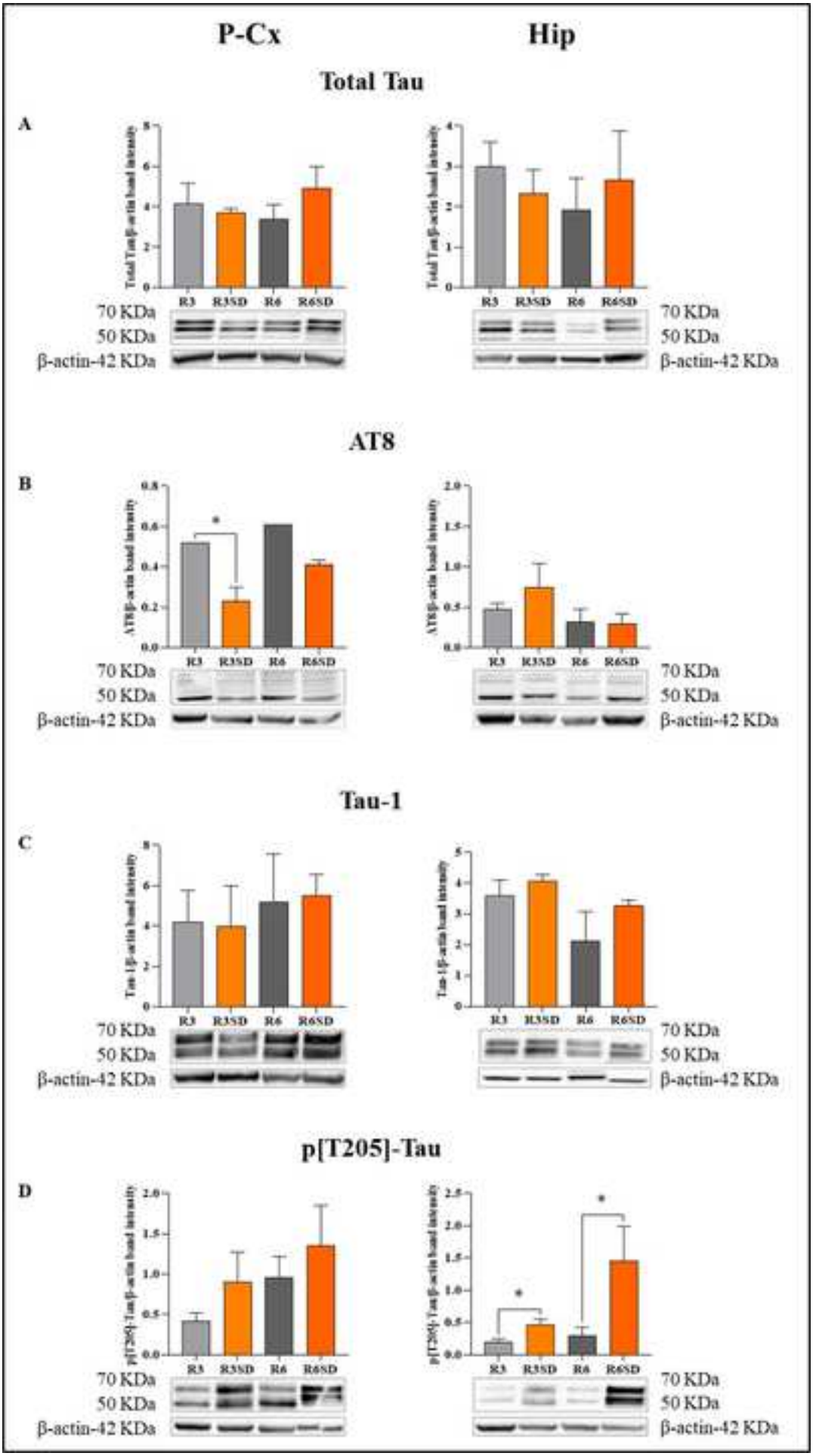

Figure 9

Click here to access/download;Figure;Hitrec-Squarcio et al_Figure 9.jpg

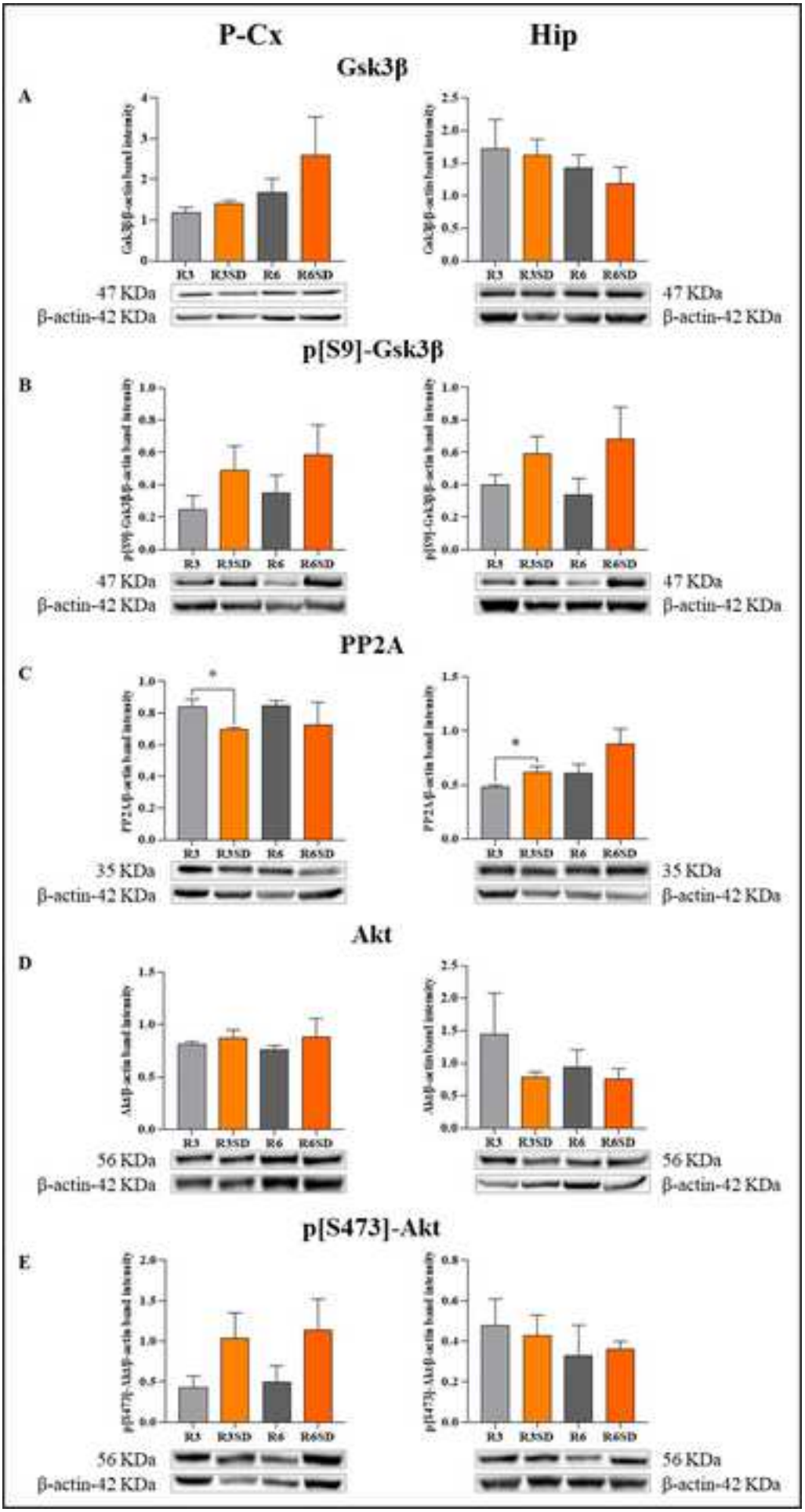

Figure 10

Click here to access/download;Figure;Hitrec-Squarcio et al_Figure 10.jpg

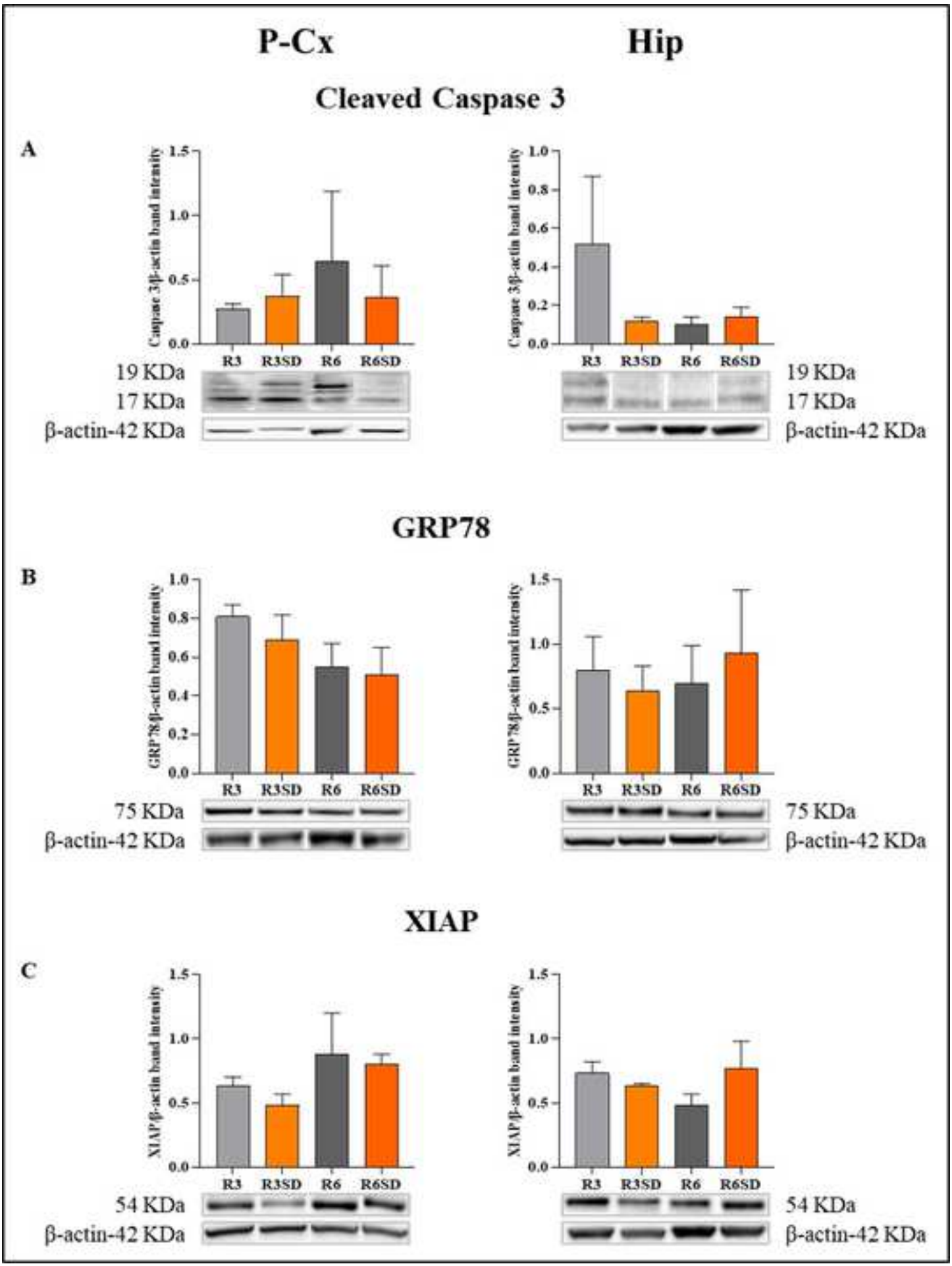

Figure 11

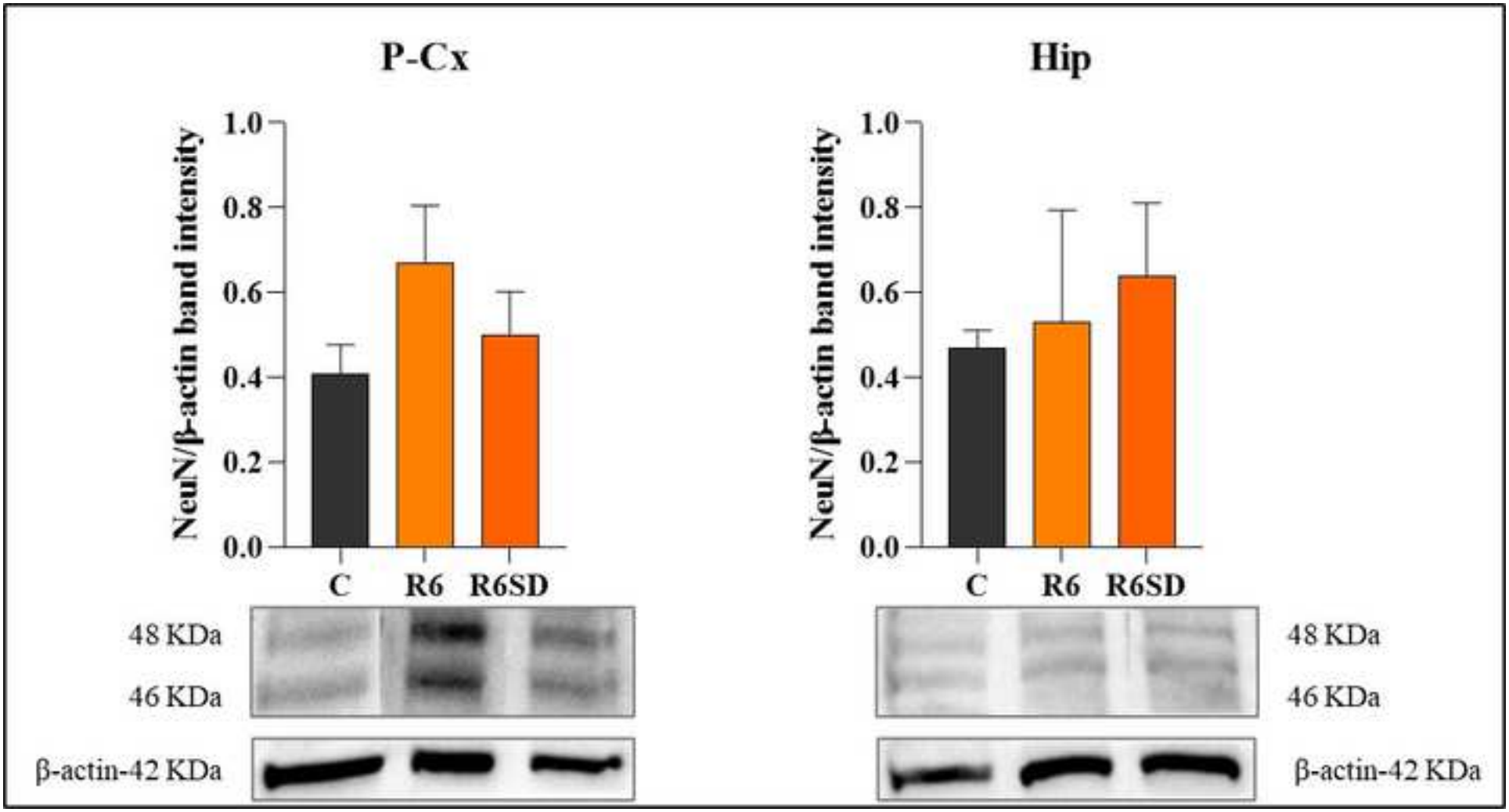

Figure 12 - corrected

Click here to access/download;Figure;Figure 12_revised.jpg

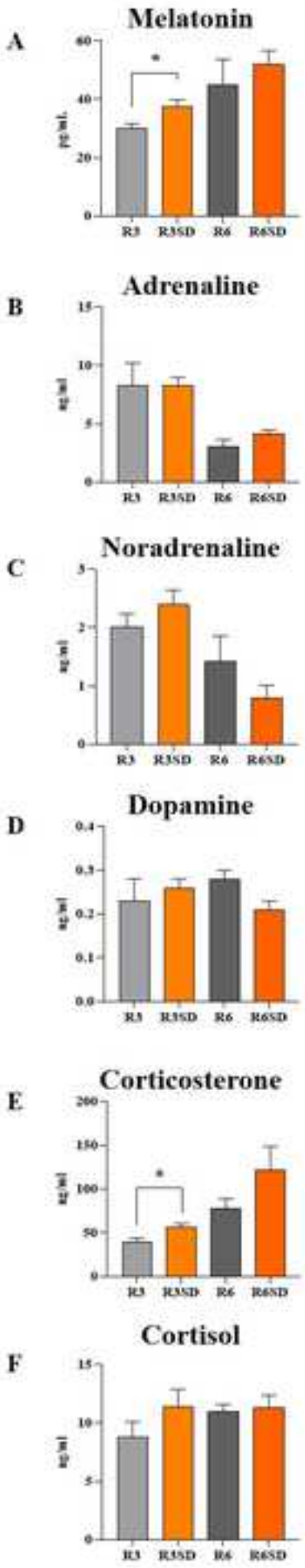

Figure 13

Click here to access/download;Figure;Hitrec-Squarcio et al_Figure 13.jpg

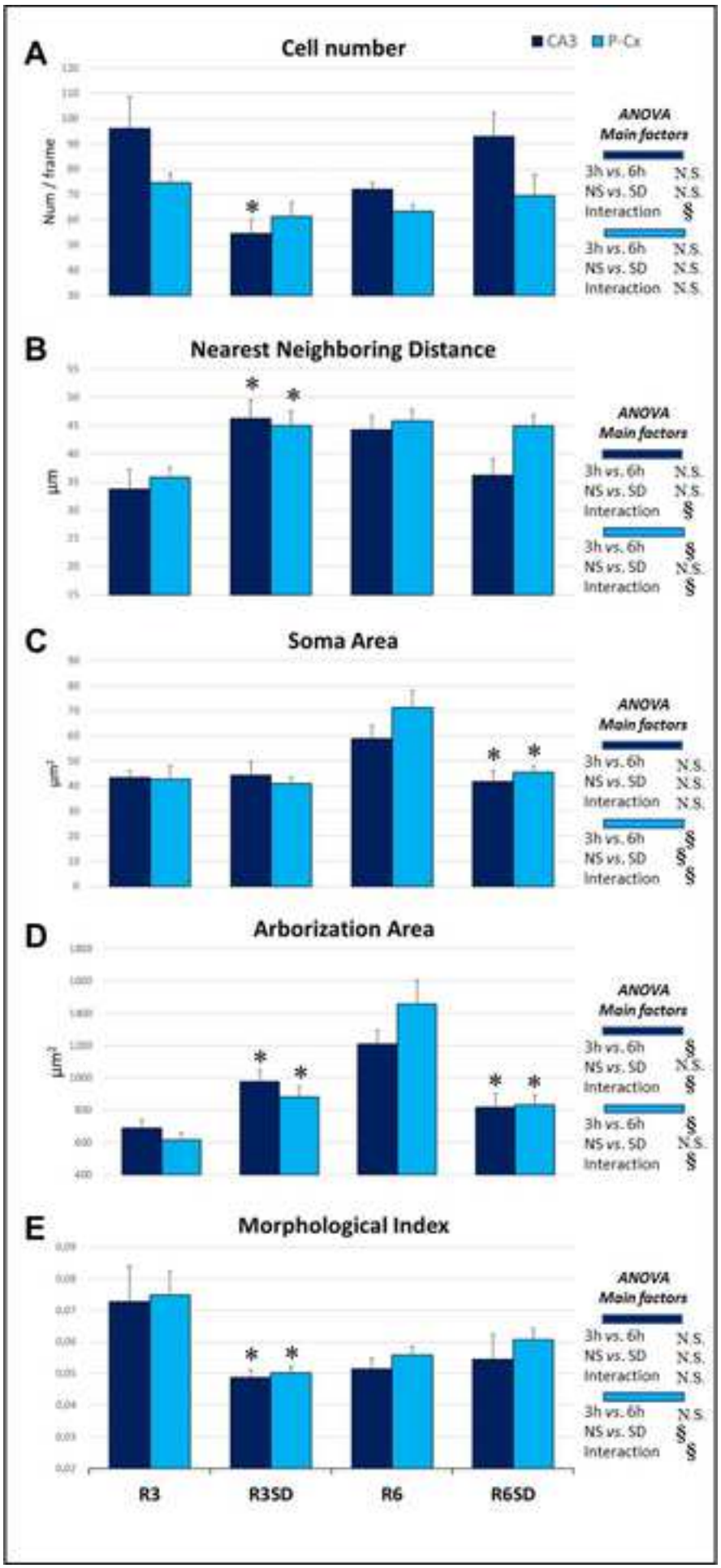

Figure 14

Click here to access/download;Figure;Hitrec-Squarcio et al_Figure 14.jpg